NEOPLASIA
www.neoplasia.com

Volume 13 Number 3 March 2011 pp. 254–265 254

Cooperation between Stat3 and Akt Signaling Leads to Prostate Tumor Development in Transgenic Mice[1,2]

Jorge M. Blando*, Steve Carbajal*, Erika Abel†, Linda Beltran*, Claudio Conti†, Susan Fischer† and John DiGiovanni*,‡

*Division of Pharmacology and Toxicology, The University of Texas at Austin, Austin, TX, USA; †Department of Molecular Carcinogenesis, The University of Texas, MD Anderson Cancer Center, Science Park – Research Division, Smithville, TX, USA; ‡Department of Nutritional Sciences, The University of Texas at Austin, Austin, TX, USA

Abstract

In this report, we describe the development of a transgenic mouse in which a rat probasin promoter (ARR_2Pb) was used to direct prostate specific expression of a constitutively active form of signal transducer and activator of transcription 3 (i.e., Stat3C). ARR_2Pb.Stat3C mice exhibited hyperplasia and prostate intraepithelial neoplasia (PIN) lesions in both ventral and dorsolateral prostate lobes at 6 and 12 months; however, no adenocarcinomas were detected. The effect of combined loss of PTEN was examined by crossing ARR_2Pb.Stat3C mice with $PTEN^{+/-}$ null mice. $PTEN^{+/-}$ null mice on an ICR genetic background developed only hyperplasia and PIN at 6 and 12 months, respectively. ARR_2Pb.Stat3C × $PTEN^{+/-}$ mice exhibited a more severe prostate phenotype compared with ARR_2Pb.Stat3C and $PTEN^{+/-}$ mice. ARR_2Pb.Stat3C × $PTEN^{+/-}$ mice developed adenocarcinomas in the ventral prostate as early as 6 months (22% incidence) that reached an incidence of 61% by 12 months. Further evaluations indicated that phospho-Stat3, phospho-Akt, phospho-nuclear factor κB, cyclin D1, and Ki67 were upregulated in adenocarcinomas from ARR_2Pb.Stat3C × $PTEN^{+/-}$ mice. In addition, membrane staining for β-catenin and E-cadherin was reduced. The changes in Stat3 and nuclear factor κB phosphorylation correlated most closely with tumor progression. Collectively, these data provide evidence that Stat3 and Akt signaling cooperate in prostate cancer development and progression and that ARR_2Pb.Stat3C × $PTEN^{+/-}$ mice represent a novel mouse model of prostate cancer to study these interactions.

Neoplasia (2011) 13, 254–265

Introduction

Signal transducers and activators of transcription (Stats) are a family of latent transcriptions factors that transmit signals from the extracellular surface of cells to the nucleus as part of the normal cellular response to cytokines and growth factors (reviewed in references [1–3]). Stats are involved in normal processes such as development, differentiation, immune function, proliferation, survival, and epithelial-to-mesenchymal transition (EMT) [1–8]. In addition, Stats have been implicated in cell growth and survival during oncogenesis. In this regard, constitutive activation of Stat3 has been observed in many human tumors including breast, prostate, melanoma, pancreas, ovarian, colorectal, and brain (reviewed in references [5–9]). In prostate cancer cell lines, Stat3 activation correlated with malignancy [10,11]. Inhibition of Stat3 in DU145 cells by antisense Stat3 oligonucleotides resulted in growth inhibition and apoptosis [10]. Stat3 has also been shown to be involved in tumor progression. Analysis of prostate adenocarcinoma specimens revealed elevated levels of activated Stat3,

Address all correspondence to: John DiGiovanni, PhD, Division of Pharmacology and Toxicology, The University of Texas at Austin, and Department of Nutritional Sciences, Dell Pediatric Research Institute, 1400 Barbara Jordan Blvd, Austin, TX 78723.
E-mail: jdigiovanni@mail.utexas.edu

[1]This study was supported by a Department of Defense Fellowship Award PC050692 (to J.B.), National Institutes of Health grants R01 CA107588 and P50 CA140388, and University of Texas MD Anderson Cancer Center Support Grant CA16672.
[2]This article refers to supplementary materials, which are designated by Figures W1 to W8 and are available online at www.neoplasia.com.
Received 24 September 2010; Revised 24 November 2010; Accepted 29 November 2010

DOI 10.1593/neo.101388

and they were positively correlated with a more advanced stage of tumors exhibiting higher Gleason scores [10]. Thus, Stat3 seems to be involved in both proliferation and survival of prostate cancer cells as well as prostate cancer progression. Our laboratory has also recently shown that overexpression of a constitutively active form of Stat3 leads to rapid progression of skin tumors associated with altered expression of markers for EMT [12,13]. These data further support a role for Stat3 in tumor progression.

Stat3 has been reported to regulate several transcription factors implicated in cell lineage determination and differentiation. In this regard, Stat3 regulates transcription factors such as Twist and the Snail family members Snail (Sna1) and Slug (Sna2) that have been shown to regulate E-cadherin expression during EMT [14–18]. Using an androgen-resistant prostate cancer cell (ARCap) model of EMT, Zhau et al. [19] demonstrated a link between LIV-1, a downstream target of Stat3, and EMT. The authors concluded that signaling through Stat3–Snail–LIV-1 resulted in an increased expression of receptor activator of nuclear factor κB (NF-κB) ligand, which facilitates bone metastases during prostate cancer progression. These studies further support the hypothesis that activated Stat3 may play a role in progression of epithelial cancers, including prostate cancer.

Tumor suppressor gene phosphatase and tensin homolog (PTEN), a lipid and protein phosphatase, is a negative regulator of AKT [20] and loss of PTEN function leads to constitutive activation of Akt [21–24]. Loss of one PTEN allele is a high-frequency event in prostate cancer, observed in up to 70% to 80% of primary tumors [24–27]. Homozygous inactivation of PTEN is associated with advanced disease and metastasis [28,29]. PTEN heterozygous null mice ($PTEN^{+/-}$ mice) develop prostate intraepithelial neoplasia (PIN) with a variable penetrance varying from 40% to 50% [30–32] to 90% [33]. Lesions develop mainly in the anterior and dorsolateral prostate but are also observed in the ventral prostate. Progression to adenocarcinoma is normally not observed in $PTEN^{+/-}$ mice, possibly related to age-dependent morbidity due to the high incidence of thymic lymphomas that occur in these mice. In contrast, conditional PTEN knockout mice with complete loss of PTEN in the prostate develop invasive prostatic carcinoma but with an extended latent period [34,35]. It has been suggested that genetic background and/or modifier genes may influence the development of lesions in PTEN-haploinsufficient animals [33]. In this regard, PTEN locus heterozygosity on a C57BL/6 genetic background seems to be fully penetrant for the development of prostate adenocarcinoma [36]. Inactivation of PTEN in combination with other mutations can promote prostate cancer progression in transgenic mice [37–40]. Studies in cancer cell lines, including prostate cancer cell lines, have shown an interaction between Stat3 and PTEN signaling pathways [41–46].

In this study, we describe the development and characterization of a transgenic mouse model (ARR_2Pb.Stat3C) in which a rat composite probasin promoter (ARR_2Pb) [47] was used to target prostate-specific expression of an activated form of Stat3 protein (Stat3C) [48]. We show that constitutive activation of Stat3 resulted in a pathologic phenotype in the prostate with the development of hyperplasia and PIN. In addition, through the generation of compound transgenic mice, we demonstrate that activation of Stat3 coupled with loss of PTEN (ARR_2Pb.Stat3C × $PTEN^{+/-}$ mice) exacerbated the prostate phenotype. Male ARR_2Pb.Stat3C × $PTEN^{+/-}$ mice developed low-grade and high-grade PIN as well as adenocarcinomas primarily in the ventral prostate. From these studies, we conclude that cooperation between Stat3 and Akt signaling pathways results in the progression from preneoplastic to neoplastic changes in the prostate of mice, resulting in the development of invasive carcinomas.

Materials and Methods

Generation of Transgenic Mice

ARR_2Pb.Stat3C transgenic line. The Stat3C complementary DNA (cDNA; courtesy of J. Bromberg) was ligated into a plasmid vector (pPB.129, courtesy of R. Mutasik) between the β-globin intron sequence and the polyadenylation signal. Expression of the Stat3C cDNA was targeted by the composite androgen-responsive probasin (ARR_2Pb) promoter to the prostate luminal epithelial cells. The recombinant vector (ARR_2Pb.Stat3C) was excised, purified using the Wizard SV DNA purification kit (Promega, Madison, WI), and used to generate transgenic founders on a FVB genetic background. Three different reactions were performed to verify full-length transgene insertion by polymerase chain reaction (PCR) using specific primers. The first reaction was performed to amplify the β-globin intron as reported previously [8], Stat3-GCC GCC GTA GTG ACA GAG AA (forward) and GGC AGC AAC ATC CCC AGA GT (reverse), the second reaction to amplify the Stat3C transgene, and the third one to amplify a fragment that contained the β-globin intron and the Stat3C transgene (β-globin intron 5′ primer and STAT3-C 3′ primer). Transgenic F1 progeny were identified by PCR amplification of genomic DNA using primers for the β-globin intron.

ARR_2Pb.Stat3C × $PTEN^{+/-}$ mice. The $PTEN^{+/-}$ line was originally received on the C57BL/6 genetic background [30]. Successive backcrosses onto ICR were performed for 10 generations before conducting this study. Mice carrying the PTEN deletion were identified by PCR of genomic DNA using the following primers: Pten (exon 5)—AGA CCA TAA CCC ACC ACA GC (forward); Pten (exon 5)—TAG GGC CTC TTG TGC CTT TA (reverse), wild-type; R1 Neo 288 (PTEN mutant)—GTG CAA TCC ATC TTG TTC AAT GGC CG (reverse) to give amplification products of ~200 bp for the wild-type and ~625 bp for the knockout. Littermates of the appropriate genotype were used for comparison in all studies. For all the studies, mice were housed in suspended polycarbonate cages or individually ventilated cages (Lab Products, Maywood, NJ) on autoclaved hardwood bedding at room temperature of 20 to 22°C, relative humidity of 60% to 70% and 14/10-hour light-dark cycle.

Histologic Analysis

For histologic analysis, the male reproductive tract was removed intact from ARR_2Pb.Stat3C, $PTEN^{+/-}$, ARR_2Pb.Stat3C × $PTEN^{+/-}$, and nontransgenic littermates at 6 and 12 months, fixed in 10% formalin, embedded in paraffin, and transversely sectioned. Sections of 4 μm were stained with hematoxylin and eosin (H&E), and immunohistochemistry (IHC) was performed on paraffin-embedded prostate tissue sections using primary antibodies against phospho-Stat3 (Tyr^{705}, 1:50), phospho-Akt (Ser^{473}, 1:50), phospho-NF-κB (p65, 1:50; Cell Signaling Technology, Beverly, MA), Flag-tag (for Stat3C, 1:50; Sigma-Aldrich, St Louis, MO), E-cadherin (1:50), Ki67 (1:50), Akt (1:100; Santa Cruz Biotechnology, Inc, Santa Cruz, CA), and β-catenin (BD Biosciences, San Jose, CA). Antibodies were detected with biotinylated secondary antibodies, followed by

Table 1. Distribution and Incidence of Prostate Lesions.

Group	Ventral Prostate			Dorsolateral Prostate		
	Hyperplasia	PIN*	AC	Hyperplasia	PIN	AC
At 6 mo						
$ARR_2Pb.Stat3C$	14/16 (88%)	5/16 (31%)	0/16 (0%)	9/16 (56%)	3/16 (18%)	0/16 (0%)
$PTEN^{+/-}$	8/8 (100%)	4/8 (50%)	0/8 (0%)	7/8 (87%)	1/8 (12%)	0/8 (0%)
$ARR_2Pb.Stat3C \times PTEN^{+/-}$	9/9 (100%)	6/9 (67%)	2/9 (22%)	9/9 (100%)	4/9 (44%)	0/9 (0%)
At 12 mo						
$ARR_2Pb.Stat3C$	25/25 (100%)	17/25 (68%)	0/25 (0%)	16/25 (61%)	11/25 (42%)	0/25 (0%)
$PTEN^{+/-}$	7/7 (100%)	5/7 (71%)	0/7 (0%)	7/7 (100%)	4/7 (57%)	0/7 (0%)
$ARR_2Pb.Stat3C \times PTEN^{+/-}$	18/18 (100%)	17/18 (94%)†	11/18 (61%)‡	18/18 (100%)	12/18 (66%)	0/18 (0%)

*AC indicates adenocarcinoma; PIN, prostatic intraepithelial neoplasia.
†Incidence of PIN was significantly different from the incidence observed in either single transgenic line ($P = .030$; Fisher exact test).
‡Incidence of AC was significantly different from the incidence observed in either single transgenic line ($P = .0001$; Fisher exact test).

peroxidase-conjugated avidin/biotin (Vectastain ABC Kit; Vector Laboratories, Burlingame, CA) and DAB substrate (Dako, Carpinteria, CA).

Western Blot Analysis

Individual prostate lobes were excised and homogenized in lysis buffer (20 mM Tris pH 7.5, 150 mM NaCl, 1 mM EDTA, 1 mM EGTA, 1% Triton X-100, 2.5 mM sodium pyrophosphate, 1 mM β-glycerophosphate, protease inhibitor cocktail [Sigma-Aldrich]). Fifty micrograms of cell lysates was electrophoretically separated on 7% to 10% SDS-PAGE and transferred onto nitrocellulose membrane (BioRad Laboratories, Hercules, CA). Transfer was performed at 30 V overnight. After blocking with 5% skim milk in phosphate-buffered saline containing 0.1% Tween, the membranes were incubated with antibodies against: flag-tag (for Stat3C, 1:1000; Sigma-Aldrich), Stat3 (1:1000), phospho-Stat3 (1:1000, Tyr^{705} and Ser^{727}), Akt (1:1000) and phospho-Akt (1:500, Thr^{308} and Ser^{473}; Cell Signaling Technology), and β-actin (mouse monoclonal, 1:4000; Sigma-Aldrich). Protein bands were detected using enhanced chemiluminescence (Pierce Biotechnology, Inc, Rockford, IL). Protein quantification was then determined using an imaging system (Alpha Innotech, Cell Biosciences, Santa Clara, CA). The relative density of each protein band was normalized to the density of the corresponding β-actin band, and where possible, phosphorylated proteins were presented as the ratio of phosphorylated and total protein.

Statistical Analyses

The incidence of prostate lesions shown in Table 1 was analyzed using the Fisher exact test. Statistical significance of data from Western blot analyses was evaluated using Wilcoxon rank-sum test. Significance was set in both cases at $P \leq .05$.

Results

$ARR_2Pb.Stat3C$ mice were generated on an FVB/N genetic background. A diagram of the DNA construct containing Stat3C cDNA used to generate the mice is shown in Figure 1*A*. Founders were screened for transgene insertion by PCR. Five founders (A, B, C, D, and E) containing the transgene were used to establish transgenic lines as described in Materials and Methods (Figure 1*B*). All but

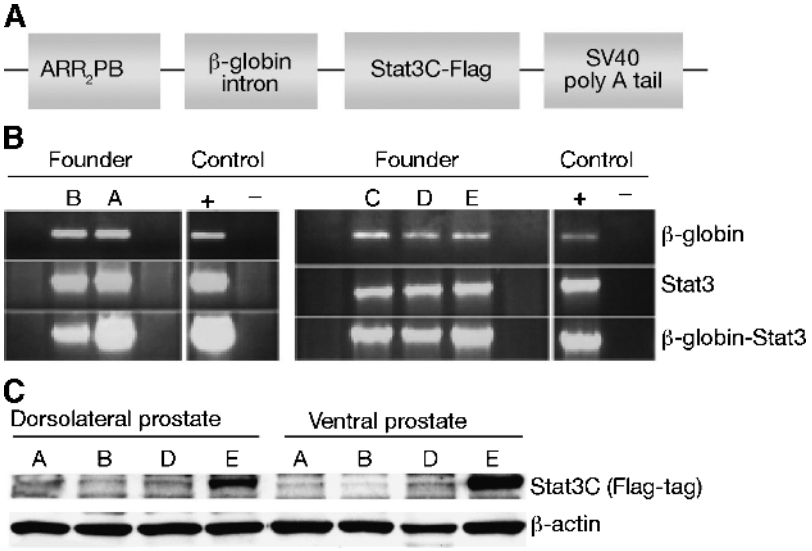

Figure 1. Verification of $ARR_2Pb.Stat3C$ transgenic founders and transgene expression. (A) Diagram of construct used to generate $ARR_2Pb.Stat3C$ founders. (B) Verification of presence of transgene by PCR analysis using sequence specific primers. (C) Western blot analysis of protein expression of Stat3C (using antibodies against the flag-tag) in lysates prepared from ventral and dorsolateral prostate. Protein was normalized to β-actin.

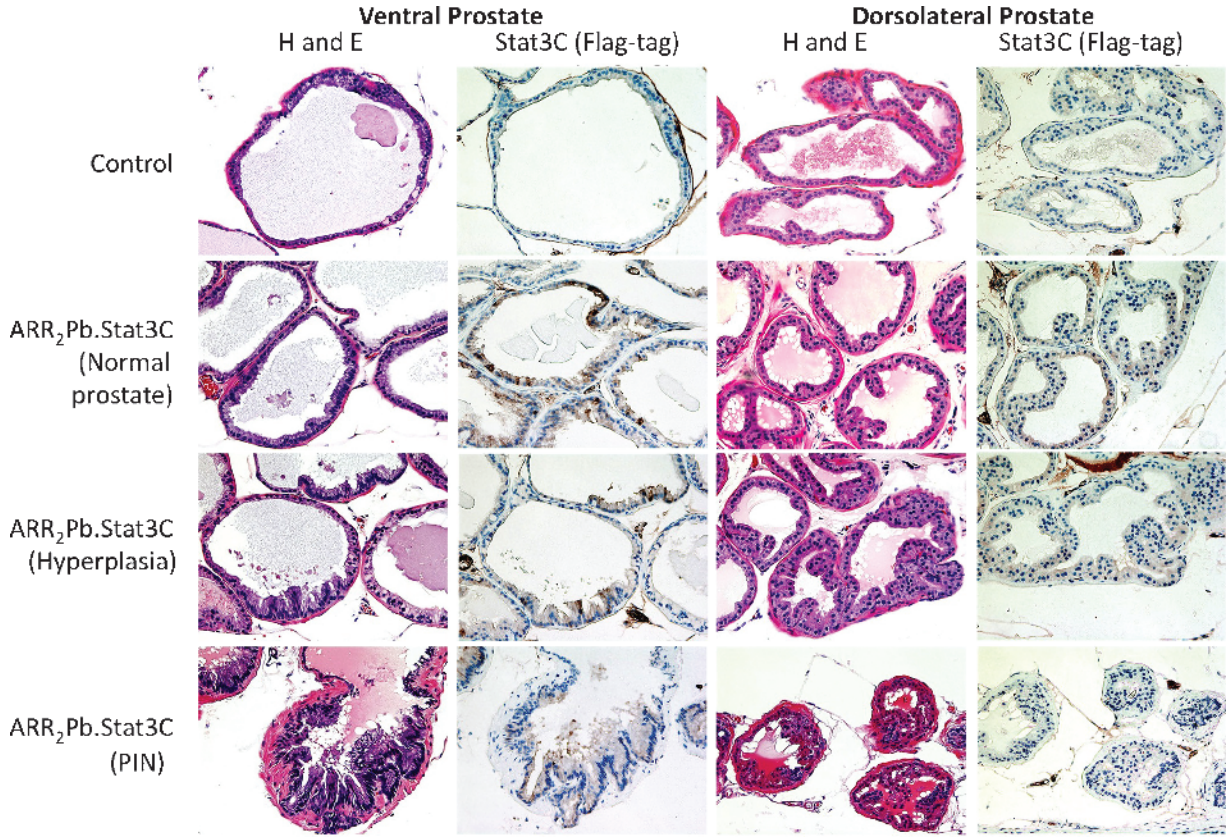

Figure 2. Characterization of prostate lesions in $ARR_2Pb.Stat3C$ male mice. H&E-stained sections and staining for transgene expression using an antibody to the flag-tag are shown in representative sections of the ventral and dorsolateral prostate lobes of $ARR_2Pb.Stat3C$ transgenic male mice. Prostates were harvested from nontransgenic (control) and $ARR_2Pb.Stat3C$ male mice at 6 or 12 months. At 6 months, prostate tissue of $ARR_2Pb.Stat3C$ transgenic mice appeared relatively normal with some areas of hyperplasia. By 12 months, lesions were more aggressive with more pronounced epithelial tufting and the development of PIN. Flag-tag expression was detected in normal (active) glands and in hyperplastic glands of the $ARR_2Pb.Stat3C$ prostate, although transgene expression appeared to be lower in PIN lesions in either prostate lobe. It should also be noted that the level of transgene expression in the dorsolateral prostate lobe was consistent with the Western blot data showing lower expression of the transgene *versus* the level observed in the ventral prostate lobe. Magnifications, ×20.

founder C passed the transgene. Protein was isolated from different lobes of the prostate of transgenic mice derived from the F1 generation of the four founders that passed the transgene, and Western blot analyses confirmed the highest level of transgene expression in mice derived from founder E (Figure 1*C*). Mice derived from founder E (i.e., line E mice) were used for all subsequent experiments.

For the morphologic characterization of the prostate, the intact reproductive tract was removed from hemizygous $ARR_2Pb.Stat3C$ male mice at both 6 (n = 16) and 12 (n = 21) months and analyzed. Histologic diagnoses of the prostate lesions were in accordance with the Consensus Report from the Bar Harbor Meeting of the Mouse Models of Human Cancer Consortium Pathology Committee [49]. As shown in Figure 2, constitutive expression of activated Stat3 resulted in a prostate phenotype characterized by hyperplasia and PIN lesions that were evident by 6 months. At 12 months, there was a 100% incidence of hyperplasia in the ventral lobe and a 61% incidence in the dorsolateral lobe. At 6 and 12 months, PIN lesions were also observed in both the ventral and dorsolateral prostate. In this regard, at 12 months, there was a 68% and 42% incidence of PIN lesions, respectively. Figures W1 and W2 show additional low- and higher-magnification H&E-stained sections of ventral prostate lesions from 12-month-old $ARR_2Pb.Stat3C$ mice. PIN lesions exhibited a cribriform pattern. In addition, cells with karyomegaly, karyocytomegaly, nuclear atypia with apical localization, and chromatin condensation were observed. The presence of one or more prominent nucleolus was also observed. To date, the development of invasive adenocarcinoma has not been observed in the $ARR_2Pb.Stat3C$ transgenic male mice on either the FVB/N or mixed FVB/N/ICR genetic background (see below).

Given that loss or inactivation of PTEN is a common occurrence in human prostate cancer [24–27] and that homozygous inactivation of PTEN is associated with advanced disease and metastasis [28,29], we examined the effect of loss of PTEN on the development of prostate lesions in $ARR_2Pb.Stat3C$ mice. Hemizygous $ARR_2Pb.Stat3C$ mice were bred to heterozygous $PTEN^{+/-}$ mice (ICR background) to generate $ARR_2Pb.Stat3C \times PTEN^{+/-}$, $ARR_2Pb.Stat3C$ and $PTEN^{+/-}$ offspring, which were then evaluated at 6 and 12 months. Note that all mice for these comparisons were littermates with the same mixed genetic background. The reproductive tract was removed and processed as described above for subsequent histologic analyses. PIN (66%) and adenocarcinoma (22%) were observed in the ventral prostate of $ARR_2Pb.Stat3C \times PTEN^{+/-}$ mice as early as 6 months. By 12 months, the incidence of PIN had increased to 94% (17/18) and the incidence of adenocarcinoma was 61% (11/18) in the ventral prostate. In contrast, adenocarcinomas were not observed in either $ARR_2Pb.Stat3C$ or

PTEN$^{+/-}$ littermates of the same age. Representative lesions from the different genotypes are shown in Figure 3 (*panel A*: 6 months; *panel B*: 12 months), and the overall incidence of prostate lesions for each genotype at 6 and 12 months is summarized in Table 1. Note that all adenocarcinomas were detected in the ventral prostate of the ARR$_2$Pb.Stat3C × PTEN$^{+/-}$ mice. Figures W3 and W4 show H&E staining of additional examples of adenocarcinomas (with higher magnifications) in the double transgenic mice. Note a clear membrane disruption of the prostate glands, stromal invasion, hemorrhage in some areas of the invaded tissue, as well as vascularization inside of the affected glands. Figure W5 shows staining for K14 which is expressed in the basal cells of the normal glands (Figure W5*A*). In adenocarcinomas (Figure W5*B*), some cells with K14 expression were also observed in the surrounding stroma. Figure W5, *C* to *E*, show laminin staining, clearly demarking areas of glandular membrane disruption.

IHC analyses were performed to assess the levels of phospho-Stat3, phospho-Akt, and cyclin D1 in lesions from the ARR$_2$Pb.Stat3C, PTEN$^{+/-}$, and ARR$_2$Pb.Stat3C × PTEN$^{+/-}$ offspring (Figure 4). Phospho-Stat3 was undetectable in PIN of ARR$_2$Pb.Stat3C mice, and although phospho-Stat3 staining was clearly evident in PIN lesions of PTEN$^{+/-}$ mice, in this case, expression was limited to the cytoplasm. In contrast, clear nuclear staining of phospho-Stat3 was evident in the PIN lesions from the ARR$_2$Pb.Stat3C × PTEN$^{+/-}$ mice, indicating activation and nuclear translocation of Stat3 in these lesions. IHC analyses of adenocarcinomas in the ARR$_2$Pb.Stat3C × PTEN$^{+/-}$ mice revealed intense nuclear staining of phospho-Stat3 (Figure 4). Total Stat3 staining was mainly observed in the cytoplasm of the PIN lesions in ARR$_2$Pb.Stat3C mice. A similar although slightly more intense staining pattern for total Stat3 was observed in the PTEN$^{+/-}$ mice and in the PIN and AC of the ARR$_2$Pb.Stat3C × PTEN$^{+/-}$ mice. Phospho-Akt staining was undetectable in PIN that developed in either the ARR$_2$Pb.Stat3C or the PTEN$^{+/-}$ mice; however, clear staining of phospho-Akt was observed in the PIN of the ARR$_2$Pb.Stat3C × PTEN$^{+/-}$, and more intense staining was observed in

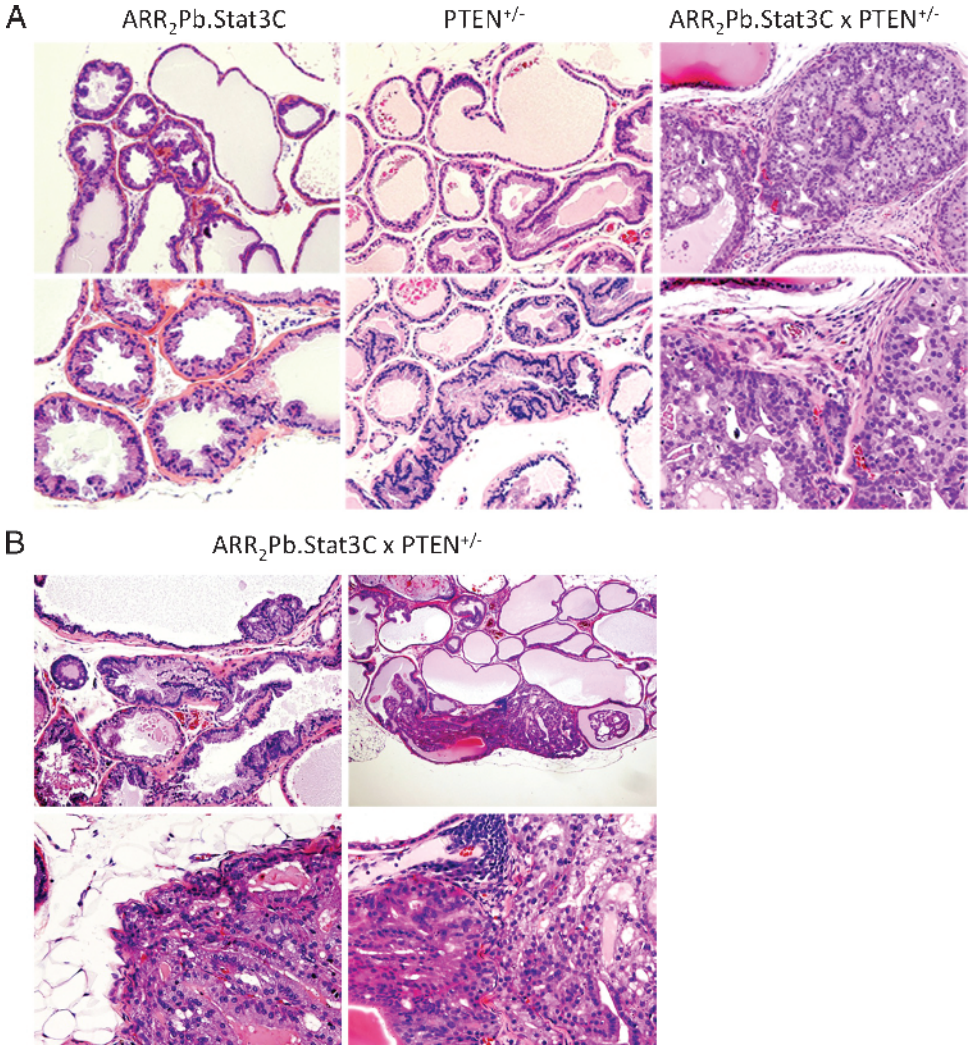

Figure 3. Characterization of prostate lesions in ARR$_2$Pb.Stat3C × PTEN$^{+/-}$ male mice. (A) Representative lesions in the ventral prostate of the ARR$_2$Pb.Stat3C, PTEN$^{+/-}$, and ARR$_2$Pb.Stat3C × PTEN$^{+/-}$ male mice at 6 months. Hyperplasia and PIN lesions developed in the ARR$_2$Pb.Stat3C and PTEN$^{+/-}$ lines, whereas in the ARR$_2$Pb.Stat3C × PTEN$^{+/-}$ transgenic mice, adenocarcinomas (AC) were observed. (B) Additional examples of hyperplasia and PIN (top left) and AC (remaining panels) in the ventral prostate of the ARR$_2$Pb.Stat3C × PTEN$^{+/-}$ mice at 12 months. ACs were characterized by disruption of the basement membrane, destructive local invasion, extension into the loose connective tissue, and foci of neovascularization.

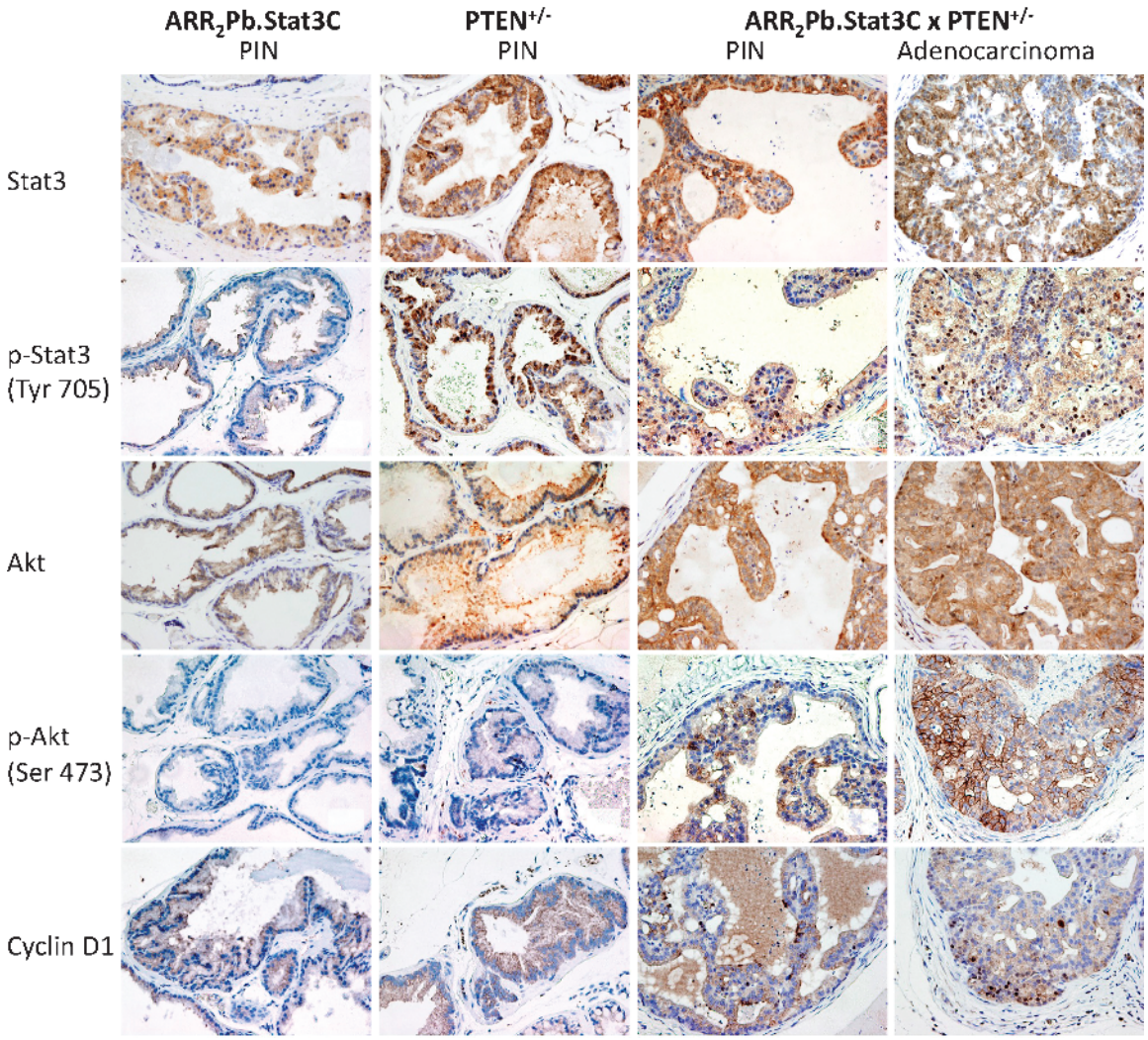

Figure 4. Status of Stat3, phospho-Stat3, Akt, phospho-Akt and Cyclin D1 in prostate of $ARR_2Pb.Stat3C \times PTEN^{+/-}$ mice. IHC analyses of the ventral prostate in the parental lines ($ARR_2Pb.Stat3C$ and $PTEN^{+/-}$) and compound transgenic mice ($ARR_2Pb.Stat3C \times PTEN^{+/-}$). All mice were aged 6 months at the time of tissue collection. IHC staining of prostate sections was performed using antibodies against Stat3, phospho-Stat3 (Tyr^{705}), Akt, phospho-Akt (Ser^{473}), and cyclin D1.

the adenocarcinomas, particularly at the membrane. Total Akt staining was mainly observed in the cytoplasm of PIN lesions in both $ARR_2Pb.Stat3C$ and $PTEN^{+/-}$ mice, whereas staining was slightly increased in PIN and AC of the $ARR_2Pb.Stat3C \times PTEN^{+/-}$ mice (again, see Figure 4). Cyclin D1 immunostaining generally followed the pattern of phospho-Stat3, that is, nuclear staining of cyclin D1 was observed in the PIN of $ARR_2Pb.Stat3C \times PTEN^{+/-}$ mice and more intense staining was observed in adenocarcinomas. In light of the finding of significant nuclear staining for phospho-Stat3 in adenocarcinomas of $ARR_2Pb.Stat3C \times PTEN^{+/-}$ mice, further analyses were performed. As shown in Figures W6 and W7, the expression of the transgene in ventral prostate of $ARR_2Pb.Stat3C$ mice (Stat3C using antibody to the flag-tag) revealed its presence and both cytoplasmic and nuclear localization in normal (active) glands and hyperplasia. However, Stat3C staining appeared lower in PIN and adenocarcinomas from $ARR_2Pb.Stat3C \times PTEN^{+/-}$ mice. In addition, little or no nuclear staining was evident. In contrast, phospho-Stat3 staining was mostly cytoplasmic in normal (active) and hyperplastic glands, but nuclear staining was evident in PIN and especially adenocarcinomas. Collectively, these results suggest that transgene expression diminished with tumor progression, whereas activation of Stat3 (presumably endogenous Stat3) increased and was associated with tumor progression in $ARR_2Pb.Stat3C \times PTEN^{+/-}$ mice.

In further experiments, Western blot analyses were performed to confirm the phosphorylation status of Stat3 and Akt in the ventral prostate of the $ARR_2Pb.Stat3C \times PTEN^{+/-}$ mice (Figure 5). For these analyses, ventral prostate tissue was collected and pooled for each genotype at 6 months. Again, all mice used for these experiments were littermates of similar mixed genetic background. Interestingly, the level of total Stat3 was comparable for each genotype, that is, similar to the level observed in the control group; however, analysis of phospho-Stat3 (both Tyr^{705} and Ser^{727}) revealed that the $ARR_2Pb.Stat3C \times PTEN^{+/-}$ mice had significantly higher ($P < .05$) levels of Stat3 phosphorylation at both sites relative to the other genotypes or nontransgenic mice. The level of total Akt protein was also relatively similar in all the groups; however, significant differences were observed in the levels of phosphorylated Akt at both the Thr^{308} and Ser^{473} phosphorylation sites. In this regard, increases in phosphorylation at both sites were observed

in the $ARR_2Pb.Stat3C$, $PTEN^{+/-}$, and the $ARR_2Pb.Stat3C \times PTEN^{+/-}$ groups relative to the level observed in the control group ($P < .05$) with the highest levels observed in the $PTEN^{+/-}$ and the $ARR_2Pb.Stat3C \times PTEN^{+/-}$ mice. The levels of Akt phosphorylation (both sites) between the $PTEN^{+/-}$ and $ARR_2Pb.Stat3C \times PTEN^{+/-}$ were not significantly different ($P > .05$). Interestingly, protein lysates from ventral prostate of $ARR_2Pb.Stat3C$ mice showed a significant increase ($P < .05$) in Akt phosphorylation (both sites) compared with control mice. Thus, overexpression of a constitutively active Stat3 either directly or indirectly led to increased phosphorylation of Akt. Overall, these results are consistent with the IHC analyses in which phospho-Stat3 and phospho-Akt were highly expressed in the adenocarcinomas of the $ARR_2Pb.Stat3C \times PTEN^{+/-}$ mice. Based on the IHC and Western blot analyses, the level of phospho-Stat3 seemed to correlate most closely with the transition from PIN to adenocarcinomas in $ARR_2Pb.Stat3C \times PTEN^{+/-}$ mice.

In light of the enhanced progression of prostate tumors observed in the $ARR_2Pb.Stat3C \times PTEN^{+/-}$ mice, we examined the expression of several other markers in ventral prostate including β-catenin, E-cadherin, and Ki67 in normal tissue, hyperplasia, PIN lesions, and adenocarcinomas by IHC. We also examined the phosphorylation status of NF-κB. The results of these analyses are shown in Figures 6 and 7. As expected, Ki67 expression was low in normal glands, whereas nuclear Ki67 expression was slightly increased in hyperplasia (Figure 6). In contrast, a significant increase in nuclear Ki67 was observed in PIN and especially adenocarcinomas. Note that Ki67 expression in the adenocarcinomas not only was present inside of the affected glands but also was observed in cells in the surrounding stroma. Immunostaining of hyperplastic tissues and PIN lesions for progression markers (i.e., β-catenin and E-cadherin) was similar to normal tissue (Figure 6). In contrast, the expression pattern of β-catenin and E-cadherin in adenocarcinomas was irregular. In some areas, there was clear loss of membrane staining for both β-catenin and E-cadherin.

As shown in Figure 7, phosphorylation of NF-κB (p65) was found in only a few scattered cells in the ventral prostate of the $ARR_2Pb.Stat3C$ and $PTEN^{+/-}$ mice. In ARR2Pb.Stat3C × $PTEN^{+/-}$ mice, there also were only few a scattered cells staining for nuclear phospho-NF-κB in nontumor areas. In contrast, there was a significant increase in nuclear staining of phospho–NF-κB (p65) in the adenocarcinomas of these mice (Figure 7, *A* and *B*). Additional adenocarcinomas from ventral prostate of the $ARR_2Pb.Stat3C \times PTEN^{+/-}$ mice were stained for phospho–NF-κB (Figure W8). As shown, all samples including those shown in Figure 7 (7/7 total, 100%) showed intense nuclear staining for phospho–NF-κB (p65). Collectively, the disruption of β-catenin

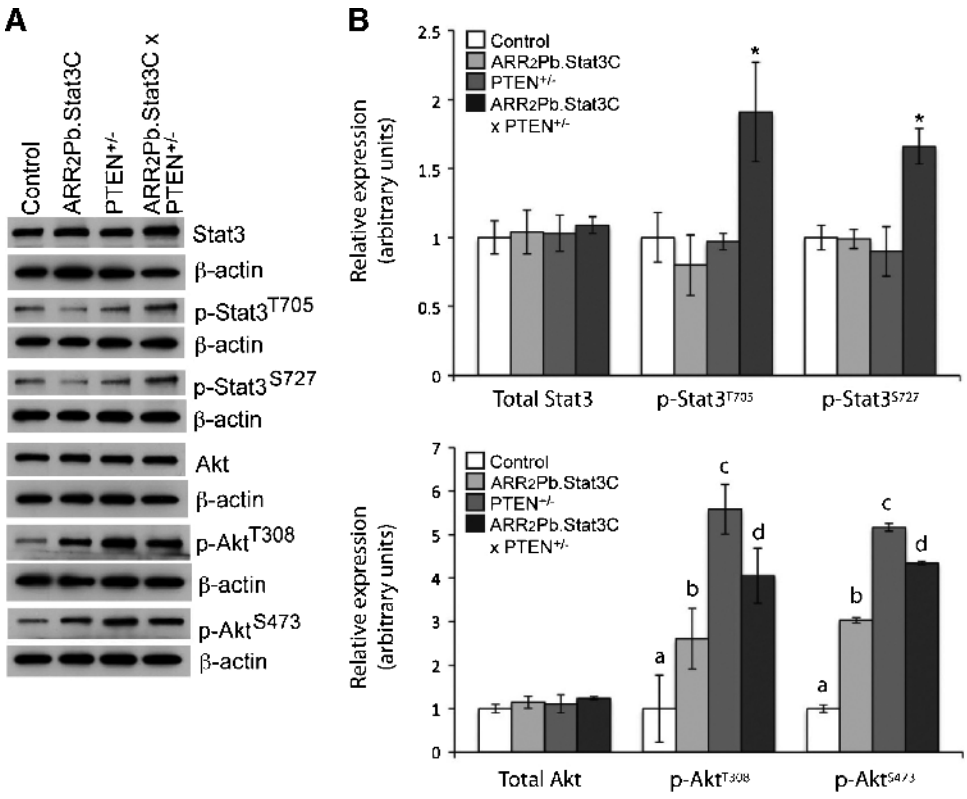

Figure 5. Western blot analyses of phosphorylation status and expression of Stat3 and Akt in ventral prostate. (A) Western blot analyses of protein lysates prepared from pooled prostate tissues from nontransgenic (control), $ARR_2Pb.Stat3C$, $PTEN^{+/-}$, and $ARR_2Pb.Stat3C \times PTEN^{+/-}$ mice using antibodies against Stat3, phospho-Stat3 (Tyr^{705} and Ser^{727}), Akt, and phospho-Akt (Thr^{308} and Ser^{473}). Mice were aged 6 months at the time of tissue collection. (B) Quantitation of protein levels by densitometry. Protein amounts were normalized using actin and levels of phosphorylated proteins are presented as the ratio of phosphorylated and total protein. (B, top panel) *Significantly different from control, $ARR_2Pb.Stat3C$, and $PTEN^{+/-}$ groups ($P < .05$, Wilcoxon rank-sum test). (B, bottom panel) [a]Significantly different from $ARR_2Pb.Stat3C$, $PTEN^{+/-}$, and $ARR_2Pb.Stat3C \times PTEN^{+/-}$ groups ($P < .05$, Wilcoxon rank-sum test). [b]Significantly different from control, $PTEN^{+/-}$, and $ARR^2Pb.Stat3C \times PTEN^{+/-}$ groups ($P < .05$, Wilcoxon rank-sum test). [c]Significantly different from control and $ARR_2Pb.Stat3C$ groups ($P < .05$, Wilcoxon rank-sum test). [d]Significantly different from control and $ARR^2Pb.Stat3C$ groups ($P < .05$, Wilcoxon rank-sum test).

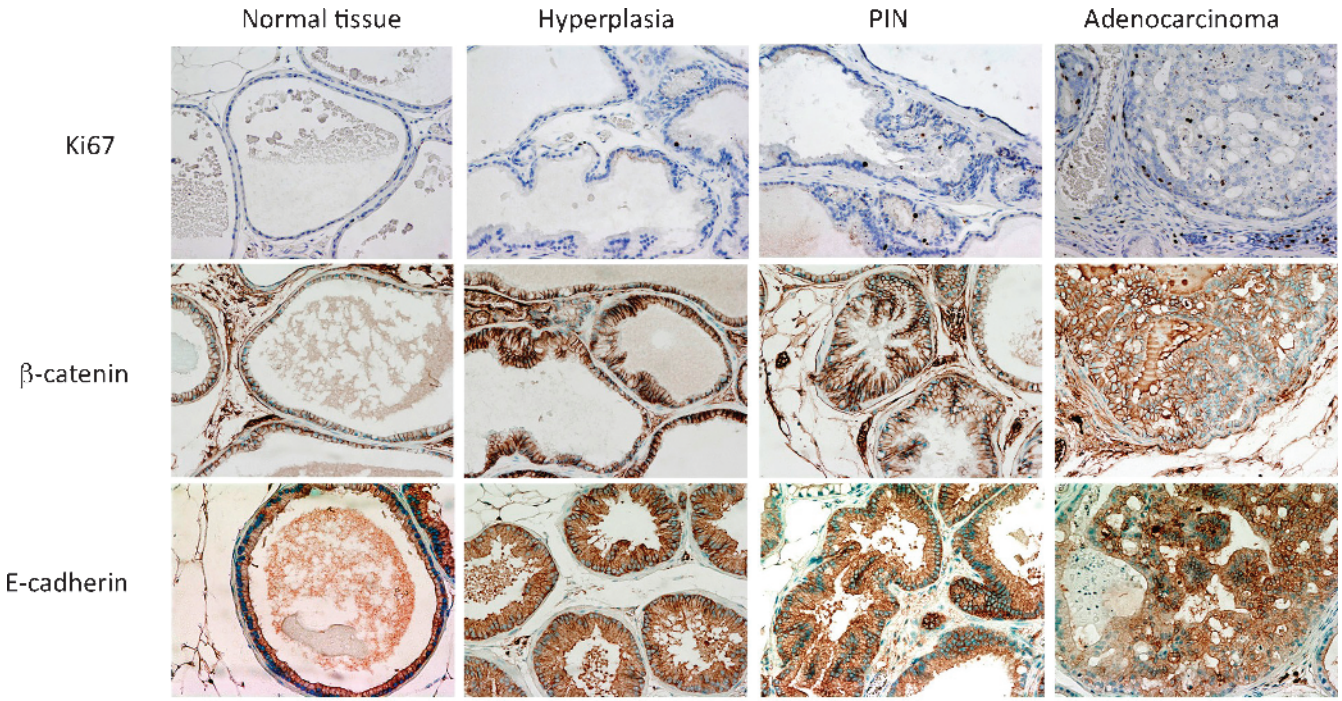

Figure 6. IHC analyses of Ki67, β-catenin, and E-cadherin in prostate of $ARR_2Pb.Stat3C \times PTEN^{+/-}$ mice. Representative stained sections of normal tissue, hyperplasia, PIN, and adenocarcinoma of the ventral prostate from $ARR_2Pb.Stat3C \times PTEN^{+/-}$ mice at 6 months are shown. IHC staining was performed using antibodies against Ki67, β-catenin, and E-cadherin as described in Materials and Methods.

and E-cadherin membrane expression and the increased expression of phospho-NF-κB also seemed to be associated with the development of adenocarcinomas and correlated with the enhanced tumor progression seen in the $ARR_2Pb.Stat3C \times PTEN^{+/-}$ mice.

Discussion

In the current study, we have described the development and characterization of a new transgenic mouse model, the $ARR_2Pb.Stat3C$ mice, in which the long probasin promoter (ARR_2Pb) was used to target prostate specific expression of an activated form of Stat3 (Stat3C). We show that expression of this constitutively active form of Stat3 resulted in a pathologic phenotype in the prostate of these mice characterized by development of hyperplasia and PIN. Furthermore, the severity and frequency of the lesions increased with age, although adenocarcinomas were not observed even in mice 1 year or older. In contrast, we showed that activation of Stat3 coupled with loss of PTEN (i.e., $ARR_2Pb.Stat3C \times PTEN^{+/-}$ mice) exacerbated the prostate phenotype compared with either $ARR_2Pb.Stat3C$ or $PTEN^{+/-}$ littermates harboring a single genetic alteration. In this regard, the $ARR_2Pb.Stat3C \times PTEN^{+/-}$ mice developed a stronger pathologic phenotype particularly in the ventral prostate. Hyperplasia (100%), PIN (67%), and adenocarcinomas (22%) were observed in the $ARR_2Pb.Stat3C \times PTEN^{+/-}$ mice as early as 6 months. At 12 months, hyperplasia was again observed in 100% of the mice, whereas PIN (94%) and adenocarcinomas (61%) were observed at a higher incidence again primarily in the ventral prostate. Thus, cross talk between Stat3 and Akt signaling pathways resulted in the progression from preneoplastic to neoplastic changes, with the outcome the development of locally invasive adenocarcinomas. IHC evaluation of adenocarcinomas from the $ARR_2Pb.Stat3C \times PTEN^{+/-}$ mice showed elevated phospho-Stat3 and phospho-Akt staining. In addition, Western blot analyses of protein lysates from ventral prostate confirmed high levels of phospho-Stat3 and phospho-Akt proteins. More intense nuclear staining of cyclin D1 and Ki67 was also observed in adenocarcinomas denoting a high proliferation rate of these lesions. Adenocarcinomas also exhibited intense nuclear staining for phospho-NF-κB (p65). Finally, β-catenin and E-cadherin expression was disrupted in adenocarcinomas consistent with the increased progression of prostate lesions.

As noted above, we found that expression of a constitutively active Stat3 (Stat3C) in mouse prostate produced exclusively premalignant lesions. Although expression of the transgene was detected in the prostate before development of premalignant lesions in $ARR_2Pb.Stat3C$ mice, transgene expression seemed to be reduced somewhat in PIN lesions (Figure 2). This reduced expression may have limited the progression of PIN to adenocarcinoma in $ARR_2Pb.Stat3C$ mice. Thus, only in the compound transgenic mice did we observe progression of PIN to adenocarcinoma. In $ARR_2Pb.Stat3C \times PTEN^{+/-}$ mice, transgene expression also seemed to be reduced in both PIN and adenocarcinomas (Figures W6 and W7). Analysis of phospho-Stat3 levels by both immunohistochemistry and Western blot revealed similar levels of both Ser^{727} and Tyr^{705} phosphorylation in ventral prostate tissue of wild-type, $ARR_2Pb.Stat3C$, and $PTEN^{+/-}$ mice but significantly elevated levels in ventral prostate of $ARR_2Pb.Stat3C \times PTEN^{+/-}$ mice at 6 months (Figure 5). This increase was presumably due to increased phosphorylation of endogenous Stat3, but we cannot rule out the possibility that both endogenous Stat3 as well as the Stat3C transgene underwent increased phosphorylation. In contrast, phospho-Akt was elevated in prostate of $ARR_2Pb.Stat3C$, $PTEN^{+/-}$, and $ARR_2Pb.Stat3C \times PTEN^{+/-}$ mice compared with wild-type mice with no statistical difference between the relative Akt phosphorylation level in the latter two genotypes (see again Figure 5). The mechanism for the increased phosphorylation of Akt in ventral prostate of $ARR_2Pb.Stat3C$ mice is

not currently known at the present time. Recently, Iliopoulos et al. [50] reported that Stat3 can regulate several microRNA, including miR21 that targets PTEN mRNA leading to reduced PTEN levels. Other mechanisms may also be involved in the increased phosphorylation of Akt in ventral prostate of ARR_2Pb.Stat3C mice and remain to be explored. Collectively, the data indicate that the combination of constitutive Stat3 activation and PTEN loss (i.e., elevated Akt) led to significant further activation of Stat3 in the ventral prostate of the compound transgenic mice. The elevated level of phospho-Stat3 observed in the ventral prostate of ARR_2Pb.Stat3C × $PTEN^{+/-}$ mice at 6 months correlated most closely with the progression of premalignant prostate lesions to adenocarcinomas.

As noted in the Introduction, Stat3 activation plays a role in prostate cancer growth and progression. Activation of Stat3 is observed in human prostate tumors and prostate cancer cell lines and seems to be involved in prostate cancer invasion and metastasis [10,11,45,51–54]. For example, an analysis of 45 adenocarcinomas obtained from radical prostatectomy showed that constitutive Stat3 activation was found in 82% of the tumors compared with matched adjacent nontumor prostate tissues. Furthermore, IHC detection of phospho-Stat3 showed that elevated Stat3 activity was localized primarily in the tumor cells of the prostate carcinoma specimens and correlated with more aggressive tumors exhibiting higher Gleason scores [10]. Stat3 is activated by phosphorylation of tyrosine and serine residues through upstream kinases. Interleukins 6 and 11 (IL-6 and IL-11) signaling has been shown to activate Stat3 in human prostate cancer and prostate cancer cell lines [52]. For example, using LNCaP, TSU, PC3, and DU145 prostate cancer cell lines, Lou et al. [51] reported an elevated growth stimulation by IL-6 accompanied by activation of Stat3 signaling. Campbell et al. [52] have shown in an *in vitro* and an *in vivo* study

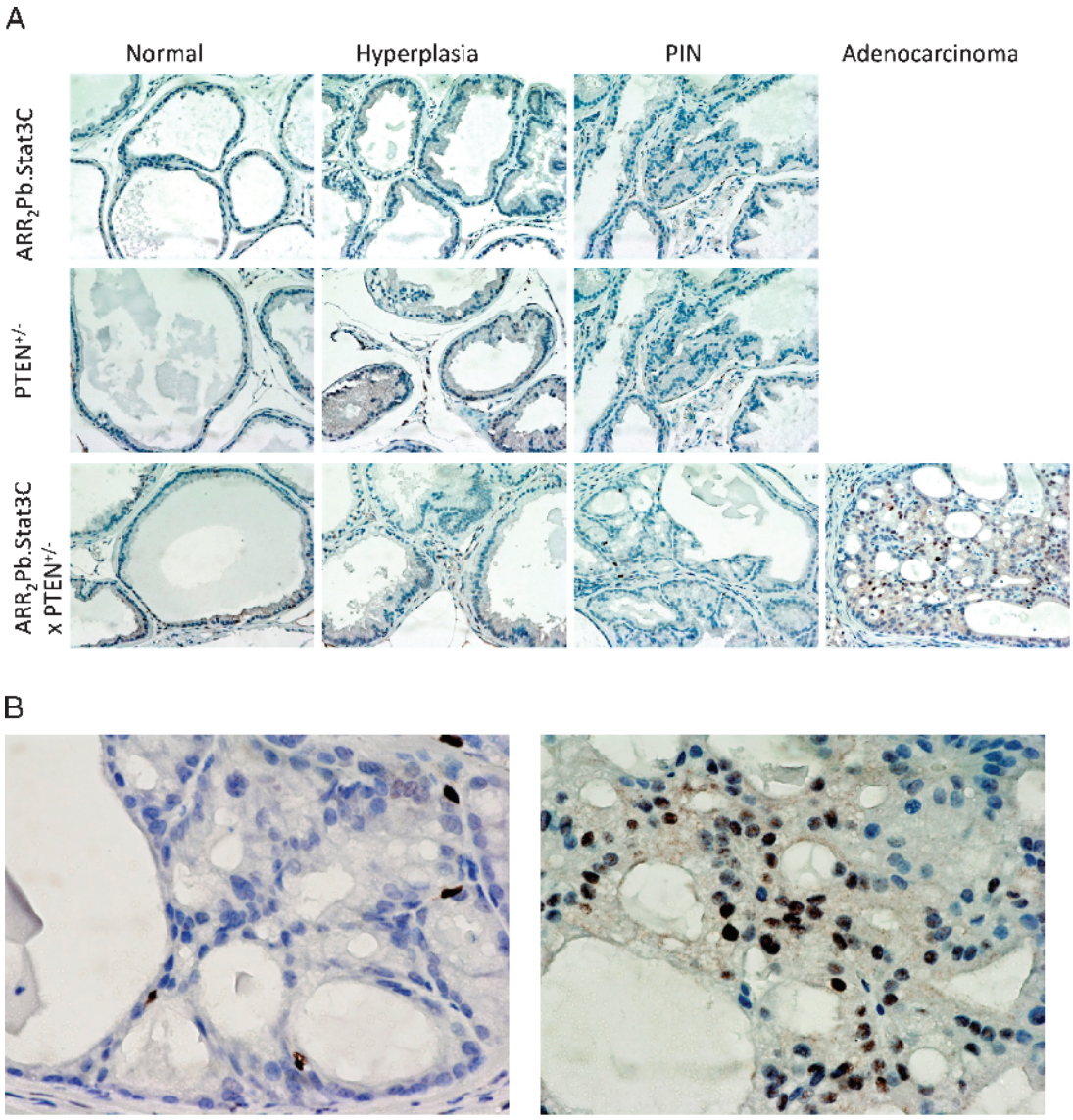

Figure 7. IHC analysis of NF-κB phosphorylation in the ventral prostate of the ARR_2Pb.Stat3C, $PTEN^{+/-}$, and ARR_2Pb.Stat3C × $PTEN^{+/-}$ transgenic mice. (A) Activated NF-κB (p65) was expressed in a small number of basal cells in normal tissue, hyperplastic, and PIN lesions in all the transgenic lines. In contrast, more intense and widespread nuclear staining was observed in adenocarcinomas from the double transgenic mice. (B) Magnification (×40) of phospho–NF-κB staining from a PIN (left) showing few cells with nuclear expression and an adenocarcinoma (right) showing a dramatic increase in the number of stained nuclei from ARR_2Pb.Stat3C × $PTEN^{+/-}$ transgenic mice.

that the IL-11 receptor system was upregulated in prostate carcinoma and that it may be one part of a cytokine network that maintains Stat3 activated in these tumors. Recently, the Fer tyrosine kinase was shown to cooperate with IL-6 to activate Stat3 in PC-3 cells [55]. The mechanism(s) whereby Stat3 activation is significantly upregulated in ventral prostate of $ARR_2Pb.Stat3C \times PTEN^{+/-}$ mice remains to be determined. One possibility could be through activation of NF-κB. As shown in Figures 7 and W8, a relatively intense nuclear staining for phospho-NF-κB was observed in adenocarcinomas from the $ARR_2Pb.Stat3C \times PTEN^{+/-}$ mice. NF-κB activation occurs as a result of PTEN loss through activation of both Akt and nitric oxide synthesis [56]. NF-κB regulates several cytokines, including IL-6 and IL-23 [56], which could lead to further activation of Stat3 in $ARR_2Pb.Stat3C \times PTEN^{+/-}$ mice. This hypothesis is currently being tested.

Further evidence for cross talk or interaction between PTEN/Akt and Stat3 signaling pathways is supported by studies in other systems. For example, Sun and Steinberg [44] reported that tyrosine phosphorylation of Stat3 (Tyr^{705}) was inversely correlated with expression of PTEN *in vitro*. Stat3 activation was found to be positively regulated with mTOR signaling, whereas PTEN served as a negative regulator of both Stat3 and mTOR signaling and was critical for cancer stem cell–like cell maintenance in MCF7 SP cells [46]. In hepatocellular carcinoma cells, a simultaneous activation of the JAK/Stat, PI3K/Akt, and Erk signaling pathways was reported to be involved in promotion of invasion and migration [43]. Although the precise mechanism(s) for interaction between these two pathways has not been clarified to date, the growing body of data suggest a clear interaction between Stat3 and Akt signaling pathways in tumor development and progression in several cancers, including prostate cancer.

Several mouse models are currently in use for the study of human prostate carcinogenesis [57–59]. Mouse models with loss of PTEN have a variety of preneoplastic and neoplastic lesions including hyperplasia, PINs, and adenocarcinomas. The development and morphology of the prostate lesions in mice with PTEN loss depend closely on the genetic background and on whether additional genetic changes are present. For example, a recent study [36] has shown that PTEN locus heterozygosity is fully penetrant for the development of prostate adenocarcinoma when present on a C57BL/6 genetic background compared with mixed genetic backgrounds [30,33] and an ICR genetic background (see Table 1; this study). The histopathologic features from normal tissue, hyperplasia, PINs to adenocarcinomas in $ARR_2Pb.Stat3C \times PTEN^{+/-}$ mice are similar to those observed in other models where PTEN loss is coupled with additional genetic alterations. For example, the prostate phenotype in the $p27Kip1^{-/-}$ mice, results only in mild hyperplasia [60–63]; however, when this mouse is crossed with the $PTEN^{+/-}$ mice ($Pten^{+/-}/Cdkn1b^{-/-}$), the lesions in the prostate glands progress to the development of adenocarcinomas in ~25% of the animals [37]. Another mouse model where PTEN loss is coupled with another genetic change is the $PTEN^{+/-} \times Nkx3.1^{-/-}$ mice. Loss of Nkx3.1 leads to hyperplasia and PIN lesions in the prostate of the mice [64]; however, when these mice are crossed with the $PTEN^{+/-}$ mice ($PTEN^{+/-} \times Nkx3.1^{-/-}$), mice develop high-grade PIN and early carcinomas [38,65]. Both of these models together with the $ARR_2Pb.Stat3C \times PTEN^{+/-}$ mouse model support the hypothesis that heterozygous PTEN loss (and thus increased PI3K/Akt signaling) cooperates with other genetic alterations to produce prostate adenocarcinomas in mice.

In conclusion, we have shown that expression of a constitutively active form of Stat3 (Stat3C) is associated with the development of premalignant prostate lesions (i.e., hyperplasia and PIN) in the ventral prostate of the ARR2Pb.Stat3C transgenic mice. Notably, when the Stat3C transgene was expressed together with loss of PTEN (i.e., $ARR2Pb.Stat3C \times PTEN^{+/-}$ mice), progression to adenocarcinomas was observed that correlated with further up-regulation of activated Stat3 (presumably endogenous Stat3) and NF-κB. These data demonstrate that cooperation between Akt and Stat3 signaling results in the development of prostate tumors in mice. We hypothesize that Stat3C transgene expression leads to early preneoplastic changes, whereas cross talk between the Stat3 signaling and Akt signaling pathways is necessary for the progression from preneoplastic to neoplastic changes in the ventral prostate of these mice. $ARR2Pb.Stat3C \times PTEN^{+/-}$ mice represent a new *in vivo* model for studying the role of Stat3 and Akt signaling in the progression of prostate cancer.

Acknowledgments

The authors thank Debra Hollowell for her excellent technical help in generating the $ARR_2Pb.Stat3C$ transgenic mice and Nancy Otto for her excellent technical assistance in the immunohistochemical staining of prostate tissue. The authors also thank Stephanie Tomlinson for her help in preparing and submitting this article for publication.

References

[1] Darnell JE Jr (1997). STATs and gene regulation. *Science* **277**, 1630–1635.
[2] Levy DE and Darnell JE Jr (2002). Stats: transcriptional control and biological impact. *Nat Rev Mol Cell Biol* **3**, 651–662.
[3] Akira S (1999). Functional roles of STAT family proteins: lessons from knockout mice. *Stem Cells* **17**, 138–146.
[4] Kisseleva T, Bhattacharya S, Braunstein J, and Schindler CW (2002). Signaling through the JAK/STAT pathway, recent advances and future challenges. *Gene* **285**, 1–24.
[5] Turkson J and Jove R (2000). STAT proteins: novel molecular targets for cancer drug discovery. *Oncogene* **19**, 6613–6626.
[6] Sano S, Itami S, Takeda K, Tarutani M, Yamaguchi Y, Miura H, Yoshikawa K, Akira S, and Takeda J (1999). Keratinocyte-specific ablation of Stat3 exhibits impaired skin remodeling, but does not affect skin morphogenesis. *EMBO J* **18**, 4657–4668.
[7] Silver DL and Montell DJ (2001). Paracrine signaling through the JAK/STAT pathway activates invasive behavior of ovarian epithelial cells in *Drosophila*. *Cell* **107**, 831–841.
[8] Sano S, Chan KS, Kira M, Kataoka K, Takagi S, Tarutani M, Itami S, Kiguchi K, Yokoi M, Sugasawa K, et al. (2005). Signal transducer and activator of transcription 3 is a key regulator of keratinocyte survival and proliferation following UV irradiation. *Cancer Res* **65**, 5720–5729.
[9] Leeman RJ, Lui VW, and Grandis JR (2006). STAT3 as a therapeutic target in head and neck cancer. *Expert Opin Biol Ther* **6**, 231–241.
[10] Mora LB, Buettner R, Seigne J, Diaz J, Ahmad N, Garcia R, Bowman T, Falcone R, Fairclough R, Cantor A, et al. (2002). Constitutive activation of Stat3 in human prostate tumors and cell lines: direct inhibition of Stat3 signaling induces apoptosis of prostate cancer cells. *Cancer Res* **62**, 6659–6666.
[11] Abdulghani J, Gu L, Dagvadorj A, Lutz J, Leiby B, Bonuccelli G, Lisanti MP, Zellweger T, Alanen K, Mirtti T, et al. (2008). Stat3 promotes metastatic progression of prostate cancer. *Am J Pathol* **172**, 1717–1728.
[12] Kim DJ, Chan KS, Sano S, and Digiovanni J (2007). Signal transducer and activator of transcription 3 (Stat3) in epithelial carcinogenesis. *Mol Carcinog* **46**, 725–731.
[13] Chan KS, Sano S, Kataoka K, Abel E, Carbajal S, Beltran L, Clifford J, Peavey M, Shen J, and Digiovanni J (2008). Forced expression of a constitutively active form of Stat3 in mouse epidermis enhances malignant progression of skin tumors induced by two-stage carcinogenesis. *Oncogene* **27**, 1087–1094.
[14] Lo HW, Hsu SC, Xia W, Cao X, Shih JY, Wei Y, Abbruzzese JL, Hortobagyi GN, and Hung MC (2007). Epidermal growth factor receptor cooperates with signal transducer and activator of transcription 3 to induce epithelial-mesenchymal transition in cancer cells via up-regulation of *TWIST* gene expression. *Cancer Res* **67**, 9066–9076.

[15] Cheng GZ, Zhang WZ, Sun M, Wang Q, Coppola D, Mansour M, Xu LM, Costanzo C, Cheng JQ, and Wang LH (2008). Twist is transcriptionally induced by activation of STAT3 and mediates STAT3 oncogenic function. *J Biol Chem* **283**, 14665–14673.

[16] Kang Y and Massague J (2004). Epithelial-mesenchymal transitions: twist in development and metastasis. *Cell* **118**, 277–279.

[17] Yang J, Mani SA, and Weinberg RA (2006). Exploring a new twist on tumor metastasis. *Cancer Res* **66**, 4549–4552.

[18] Peinado H, Olmeda D, and Cano A (2007). Snail, Zeb and bHLH factors in tumour progression: an alliance against the epithelial phenotype? *Nat Rev Cancer* **7**, 415–428.

[19] Zhau HE, Odero-Marah V, Lue HW, Nomura T, Wang R, Chu G, Liu ZR, Zhou BP, Huang WC, and Chung LW (2008). Epithelial to mesenchymal transition (EMT) in human prostate cancer: lessons learned from ARCaP model. *Clin Exp Metastasis* **25**, 601–610.

[20] Steck PA, Pershouse MA, Jasser SA, Yung WK, Lin H, Ligon AH, Langford LA, Baumgard ML, Hattier T, Davis T, et al. (1997). Identification of a candidate tumour suppressor gene, *MMAC1*, at chromosome 10q23.3 that is mutated in multiple advanced cancers. *Nat Genet* **15**, 356–362.

[21] Altomare DA and Testa JR (2005). Perturbations of the AKT signaling pathway in human cancer. *Oncogene* **24**, 7455–7464.

[22] Shaw RJ and Cantley LC (2006). Ras, PI(3)K and mTOR signalling controls tumour cell growth. *Nature* **441**, 424–430.

[23] Vivanco I and Sawyers CL (2002). The phosphatidylinositol 3-kinase AKT pathway in human cancer. *Nat Rev Cancer* **2**, 489–501.

[24] Hay N (2005). The Akt-mTOR tango and its relevance to cancer. *Cancer Cell* **8**, 179–183.

[25] Cully M, You H, Levine AJ, and Mak TW (2006). Beyond PTEN mutations: the PI3K pathway as an integrator of multiple inputs during tumorigenesis. *Nat Rev Cancer* **6**, 184–192.

[26] Sulis ML and Parsons R (2003). PTEN: from pathology to biology. *Trends Cell Biol* **13**, 478–483.

[27] Eng C (2003). *PTEN*: one gene, many syndromes. *Hum Mutat* **22**, 183–198.

[28] Cantley LC and Neel BG (1999). New insights into tumor suppression: PTEN suppresses tumor formation by restraining the phosphoinositide 3-kinase/AKT pathway. *Proc Natl Acad Sci USA* **96**, 4240–4245.

[29] Di Cristofano A and Pandolfi PP (2000). The multiple roles of PTEN in tumor suppression. *Cell* **100**, 387–390.

[30] Podsypanina K, Ellenson LH, Nemes A, Gu J, Tamura M, Yamada KM, Cordon-Cardo C, Catoretti G, Fisher PE, and Parsons R (1999). Mutation of Pten/Mmac1 in mice causes neoplasia in multiple organ systems. *Proc Natl Acad Sci USA* **96**, 1563–1568.

[31] Di Cristofano A, Pesce B, Cordon-Cardo C, and Pandolfi PP (1998). Pten is essential for embryonic development and tumour suppression. *Nat Genet* **19**, 348–355.

[32] Stambolic V, Tsao MS, Macpherson D, Suzuki A, Chapman WB, and Mak TW (2000). High incidence of breast and endometrial neoplasia resembling human Cowden syndrome in pten+/– mice. *Cancer Res* **60**, 3605–3611.

[33] Freeman D, Lesche R, Kertesz N, Wang S, Li G, Gao J, Groszer M, Martinez-Diaz H, Rozengurt N, Thomas G, et al. (2006). Genetic background controls tumor development in PTEN-deficient mice. *Cancer Res* **66**, 6492–6496.

[34] Backman SA, Ghazarian D, So K, Sanchez O, Wagner KU, Hennighausen L, Suzuki A, Tsao MS, Chapman WB, Stambolic V, et al. (2004). Early onset of neoplasia in the prostate and skin of mice with tissue-specific deletion of Pten. *Proc Natl Acad Sci USA* **101**, 1725–1730.

[35] Trotman LC, Niki M, Dotan ZA, Koutcher JA, Di Cristofano A, Xiao A, Khoo AS, Roy-Burman P, Greenberg NM, Van Dyke T, et al. (2003). Pten dose dictates cancer progression in the prostate. *PLoS Biol* **1**, E59.

[36] Blando J, Portis M, Benavides F, Alexander A, Mills G, Dave B, Conti CJ, Kim J, and Walker CL (2009). PTEN deficiency is fully penetrant for prostate adenocarcinoma in C57BL/6 mice via mTOR-dependent growth. *Am J Pathol* **174**, 1869–1879.

[37] Di Cristofano A, De Acetis M, Koff A, Cordon-Cardo C, and Pandolfi PP (2001). Pten and $p27^{KIP1}$ cooperate in prostate cancer tumor suppression in the mouse. *Nat Genet* **27**, 222–224.

[38] Kim MJ, Cardiff RD, Desai N, Banach-Petrosky WA, Parsons R, Shen MM, and Abate-Shen C (2002). Cooperativity of Nkx3.1 and Pten loss of function in a mouse model of prostate carcinogenesis. *Proc Natl Acad Sci USA* **99**, 2884–2889.

[39] Abate-Shen C, Banach-Petrosky WA, Sun X, Economides KD, Desai N, Gregg JP, Borowsky AD, Cardiff RD, and Shen MM (2003). Nkx3.1;Pten mutant mice develop invasive prostate adenocarcinoma and lymph node metastases. *Cancer Res* **63**, 3886–3890.

[40] Chen Z, Trotman LC, Shaffer D, Lin HK, Dotan ZA, Niki M, Koutcher JA, Scher HI, Ludwig T, Gerald W, et al. (2005). Crucial role of p53-dependent cellular senescence in suppression of Pten-deficient tumorigenesis. *Nature* **436**, 725–730.

[41] Godoy-Tundidor S, Cavarretta IT, Fuchs D, Fiechtl M, Steiner H, Friedbichler K, Bartsch G, Hobisch A, and Culig Z (2005). Interleukin-6 and oncostatin M stimulation of proliferation of prostate cancer 22Rv1 cells through the signaling pathways of p38 mitogen-activated protein kinase and phosphatidylinositol 3-kinase. *Prostate* **64**, 209–216.

[42] Lin DL, Whitney MC, Yao Z, and Keller ET (2001). Interleukin-6 induces androgen responsiveness in prostate cancer cells through up-regulation of androgen receptor expression. *Clin Cancer Res* **7**, 1773–1781.

[43] Saxena NK, Sharma D, Ding X, Lin S, Marra F, Merlin D, and Anania FA (2007). Concomitant activation of the JAK/STAT, PI3K/AKT, and ERK signaling is involved in leptin-mediated promotion of invasion and migration of hepatocellular carcinoma cells. *Cancer Res* **67**, 2497–2507.

[44] Sun S and Steinberg BM (2002). PTEN is a negative regulator of STAT3 activation in human papillomavirus–infected cells. *J Gen Virol* **83**, 1651–1658.

[45] Yang L, Wang L, Lin HK, Kan PY, Xie S, Tsai MY, Wang PH, Chen YT, and Chang C (2003). Interleukin-6 differentially regulates androgen receptor transactivation via PI3K-Akt, STAT3, and MAPK, three distinct signal pathways in prostate cancer cells. *Biochem Biophys Res Commun* **305**, 462–469.

[46] Zhou J, Wulfkuhle J, Zhang H, Gu P, Yang Y, Deng J, Margolick JB, Liotta LA, Petricoin E III, and Zhang Y (2007). Activation of the PTEN/mTOR/STAT3 pathway in breast cancer stem–like cells is required for viability and maintenance. *Proc Natl Acad Sci USA* **104**, 16158–16163.

[47] Zhang J, Thomas TZ, Kasper S, and Matusik RJ (2000). A small composite probasin promoter confers high levels of prostate-specific gene expression through regulation by androgens and glucocorticoids *in vitro* and *in vivo*. *Endocrinology* **141**, 4698–4710.

[48] Bromberg JF, Wrzeszczynska MH, Devgan G, Zhao Y, Pestell RG, Albanese C, and Darnell JE Jr (1999). *Stat3* as an oncogene. *Cell* **98**, 295–303.

[49] Shappell SB, Thomas GV, Roberts RL, Herbert R, Ittmann MM, Rubin MA, Humphrey PA, Sundberg JP, Rozengurt N, Barrios R, et al. (2004). Prostate pathology of genetically engineered mice: definitions and classification. The consensus report from the Bar Harbor meeting of the Mouse Models of Human Cancer Consortium Prostate Pathology Committee. *Cancer Res* **64**, 2270–2305.

[50] Iliopoulos D, Jaeger SA, Hirsch HA, Bulyk ML, and Struhl K (2010). STAT3 activation of miR-21 and miR-181b-1 via PTEN and CYLD are part of the epigenetic switch linking inflammation to cancer. *Mol Cell* **39**, 493–506.

[51] Lou W, Ni Z, Dyer K, Tweardy DJ, and Gao AC (2000). Interleukin-6 induces prostate cancer cell growth accompanied by activation of stat3 signaling pathway. *Prostate* **42**, 239–242.

[52] Campbell CL, Jiang Z, Savarese DM, and Savarese TM (2001). Increased expression of the interleukin-11 receptor and evidence of STAT3 activation in prostate carcinoma. *Am J Pathol* **158**, 25–32.

[53] DeMiguel F, Lee SO, Lou W, Xiao X, Pflug BR, Nelson JB, and Gao AC (2002). Stat3 enhances the growth of LNCaP human prostate cancer cells in intact and castrated male nude mice. *Prostate* **52**, 123–129.

[54] Dhir R, Ni Z, Lou W, DeMiguel F, Grandis JR, and Gao AC (2002). Stat3 activation in prostatic carcinomas. *Prostate* **51**, 241–246.

[55] Zoubeidi A, Rocha J, Zouanat FZ, Hamel L, Scarlata E, Aprikian AG, and Chevalier S (2009). The Fer tyrosine kinase cooperates with interleukin-6 to activate signal transducer and activator of transcription 3 and promote human prostate cancer cell growth. *Mol Cancer Res* **7**, 142–155.

[56] Grivennikov S, Karin E, Terzic J, Mucida D, Yu GY, Vallabhapurapu S, Scheller J, Rose-John S, Cheroutre H, Eckmann L, et al. (2009). IL-6 and Stat3 are required for survival of intestinal epithelial cells and development of colitis-associated cancer. *Cancer Cell* **15**, 103–113.

[57] Abdulkadir SA and Kim J (2005). Genetically engineered murine models of prostate cancer: insights into mechanisms of tumorigenesis and potential utility. *Future Oncol* **1**, 351–360.

[58] Powell WC, Cardiff RD, Cohen MB, Miller GJ, and Roy-Burman P (2003). Mouse strains for prostate tumorigenesis based on genes altered in human prostate cancer. *Curr Drug Targets* **4**, 263–279.

[59] Kasper S (2005). Survey of genetically engineered mouse models for prostate cancer: analyzing the molecular basis of prostate cancer development, progression, and metastasis. *J Cell Biochem* **94**, 279–297.

[60] Cordon-Cardo C, Koff A, Drobnjak M, Capodieci P, Osman I, Millard SS, Gaudin PB, Fazzari M, Zhang ZF, Massague J, et al. (1998). Distinct altered patterns of $p27^{KIP1}$ gene expression in benign prostatic hyperplasia and prostatic carcinoma. *J Natl Cancer Inst* **90**, 1284–1291.

[61] Fero ML, Rivkin M, Tasch M, Porter P, Carow CE, Firpo E, Polyak K, Tsai LH, Broudy V, Perlmutter RM, et al. (1996). A syndrome of multiorgan hyperplasia with features of gigantism, tumorigenesis, and female sterility in p27(Kip1)-deficient mice. *Cell* **85**, 733–744.

[62] Kiyokawa H, Kineman RD, Manova-Todorova KO, Soares VC, Hoffman ES, Ono M, Khanam D, Hayday AC, Frohman LA, and Koff A (1996). Enhanced growth of mice lacking the cyclin-dependent kinase inhibitor function of p27(Kip1). *Cell* **85**, 721–732.

[63] Nakayama K, Ishida N, Shirane M, Inomata A, Inoue T, Shishido N, Horii I, and Loh DY (1996). Mice lacking p27(Kip1) display increased body size, multiple organ hyperplasia, retinal dysplasia, and pituitary tumors. *Cell* **85**, 707–720.

[64] Schneider A, Brand T, Zweigerdt R, and Arnold H (2000). Targeted disruption of the Nkx3.1 gene in mice results in morphogenetic defects of minor salivary glands: parallels to glandular duct morphogenesis in prostate. *Mech Dev* **95**, 163–174.

[65] Kim MJ, Bhatia-Gaur R, Banach-Petrosky WA, Desai N, Wang Y, Hayward SW, Cunha GR, Cardiff RD, Shen MM, and Abate-Shen C (2002). Nkx3.1 mutant mice recapitulate early stages of prostate carcinogenesis. *Cancer Res* **62**, 2999–3004.

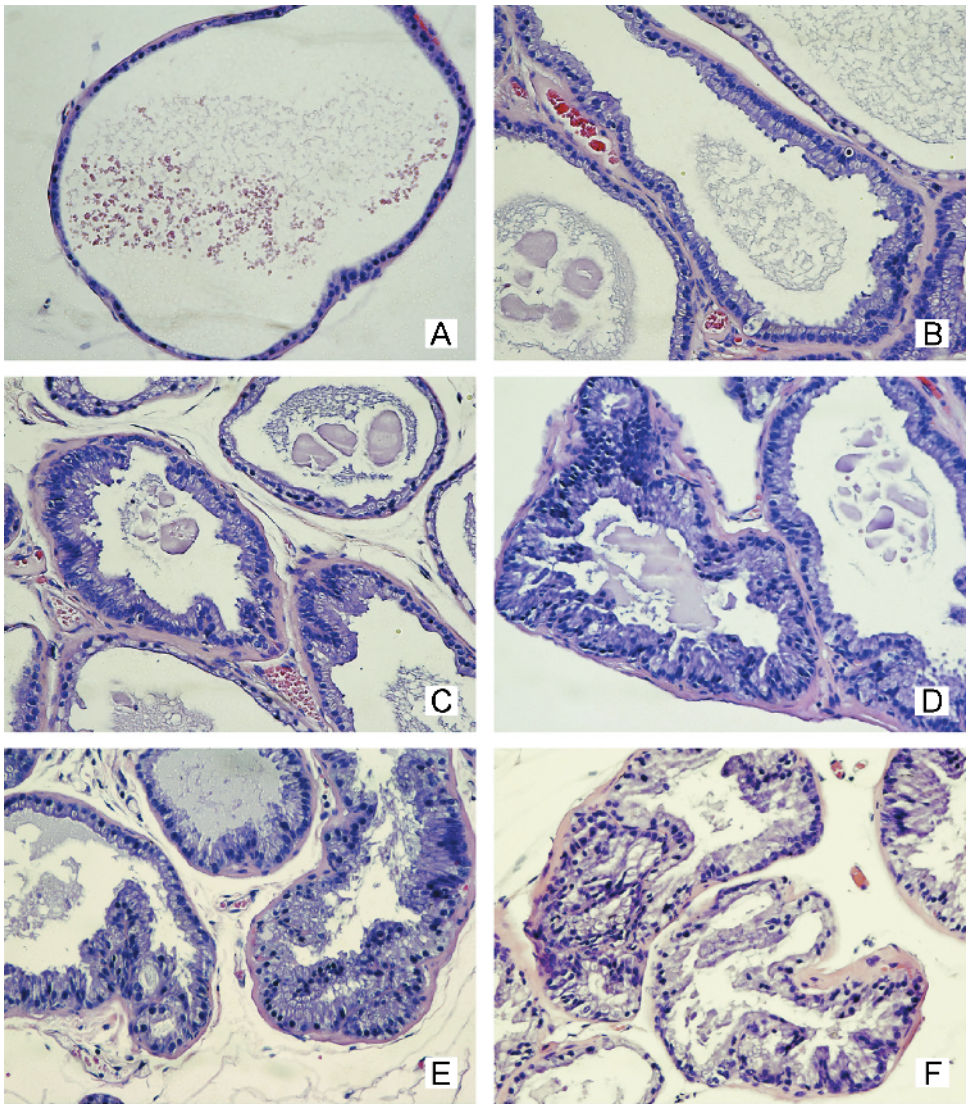

Figure W1. H&E-stained sections of the ventral prostate from $ARR_2Pb.Stat3C$ mice at 12 months. Areas of normal tissue, hyperplasia, and PIN lesions are shown. (A and B) Ventral prostate showing a single stratum of luminal epithelial cells with normal flat morphology for quiescent glands (A) and typical cells with cylindrical shape in an active epithelium (B). (C and D) Ventral prostate from a 12-month-old mouse showing luminal epithelial hyperplasia without cellular atypia (C) and with cellular atypia (D). The hyperplasia was characterized by an increase in epithelial tufting but otherwise the appearance of the cells was relatively normal. (E and F) PIN lesions were characterized by cell enlargement, karyomegaly, karyocytomegaly, nuclear atypia with apical localization, chromatin condensation, and the presence of one or more prominent nucleoli. Also, a cribriform growth pattern, as well as the formation of many small intraluminal glands, was noted. Magnifications, $\times 10$.

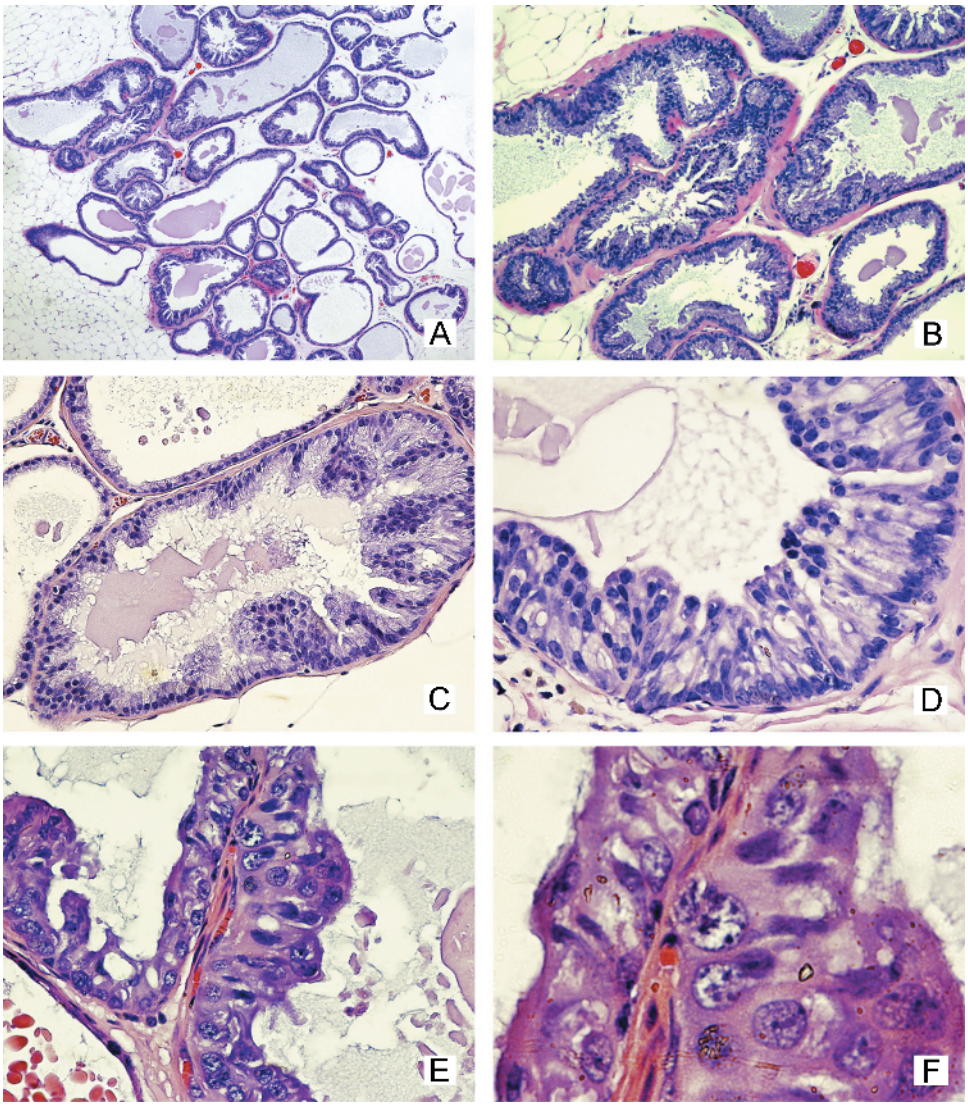

Figure W2. Additional H&E-stained sections of lesions in the ventral prostate from ARR_2Pb.Stat3C mice. (A and B) Areas of the ventral prostate with mixed normal tissue and PINs with fusiform and cribriform patterns (4×). (C and D) The ×10 and ×20 magnifications of a PIN lesion. Note that the nucleus in cells of this PIN lesion are adopting an apical position compared with a more basal position in the normal cells. (E and F) Higher magnification (×40 and ×100) of the PIN lesions in the VP. This section shows the variety of shapes of the dysplastic nuclei and cells. Cells also presented with karyocytomegaly and an increase in number and size of the nucleolus. Note the difference in the sizes of the nucleolus among cells as well as chromatin condensation and nuclear atypia.

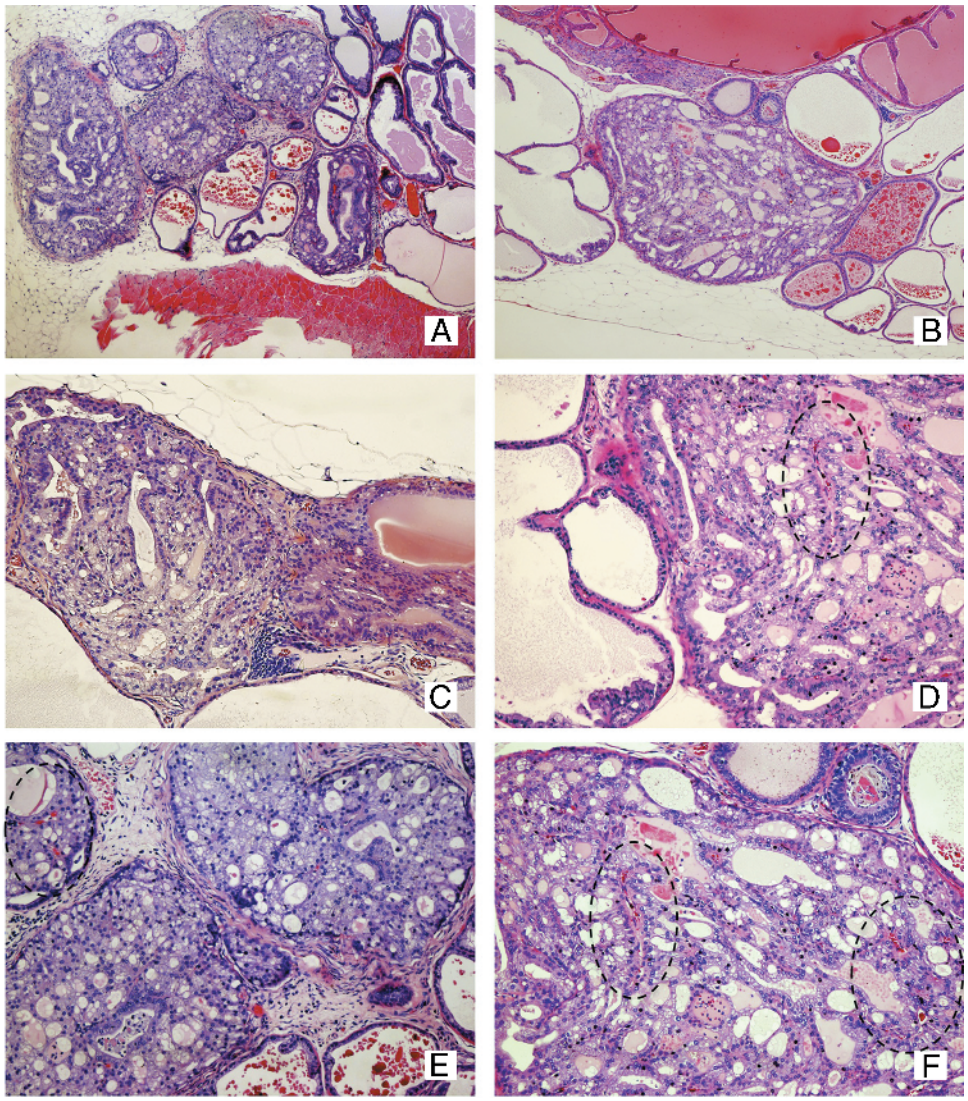

Figure W3. Additional examples of invasive adenocarcinomas in the ventral prostate of double transgenic ($ARR_2Pb.Stat3C \times PTEN^{+/-}$) mice. (A and B) Adenocarcinomas from the ventral prostate of a 12-month-old $ARR_2Pb.Stat3C \times PTEN^{+/-}$ mouse. Note the widespread local invasion of moderate- to well-differentiated tumor cells (×4). (C–F) Higher magnifications (×10) of adenocarcinomas from the ventral. Circles in panels D, E, and F show areas of neovascularization inside of the neoplastic gland.

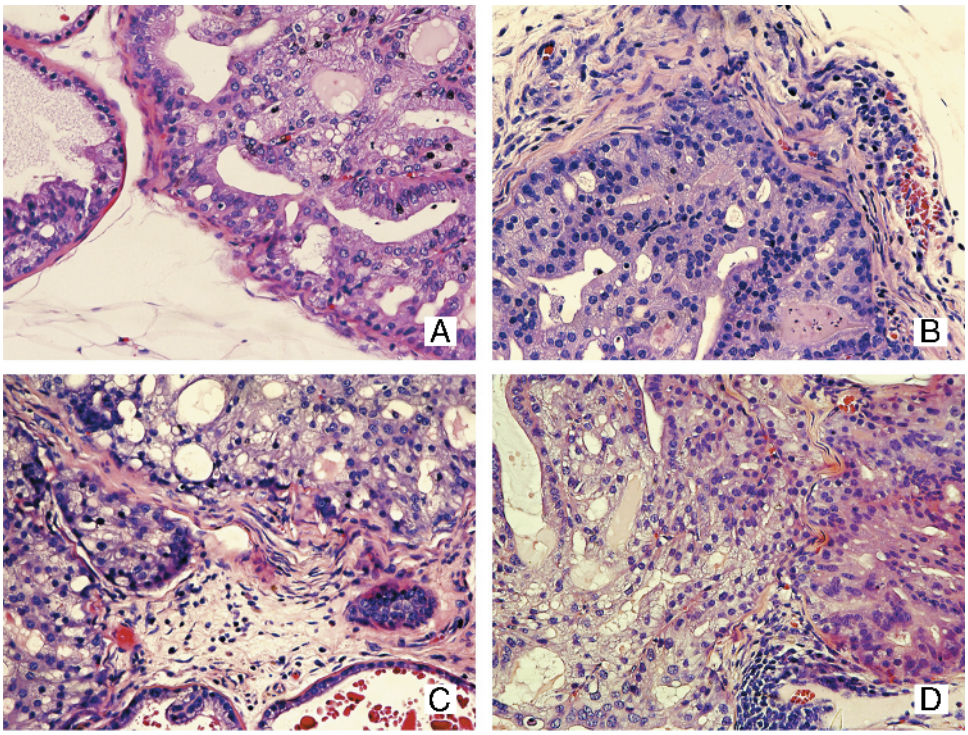

Figure W4. (A–D) Additional examples (larger magnification) of neoplastic glands with clear membrane disruption and stromal invasion. Note also the formation of small intraluminal glands.

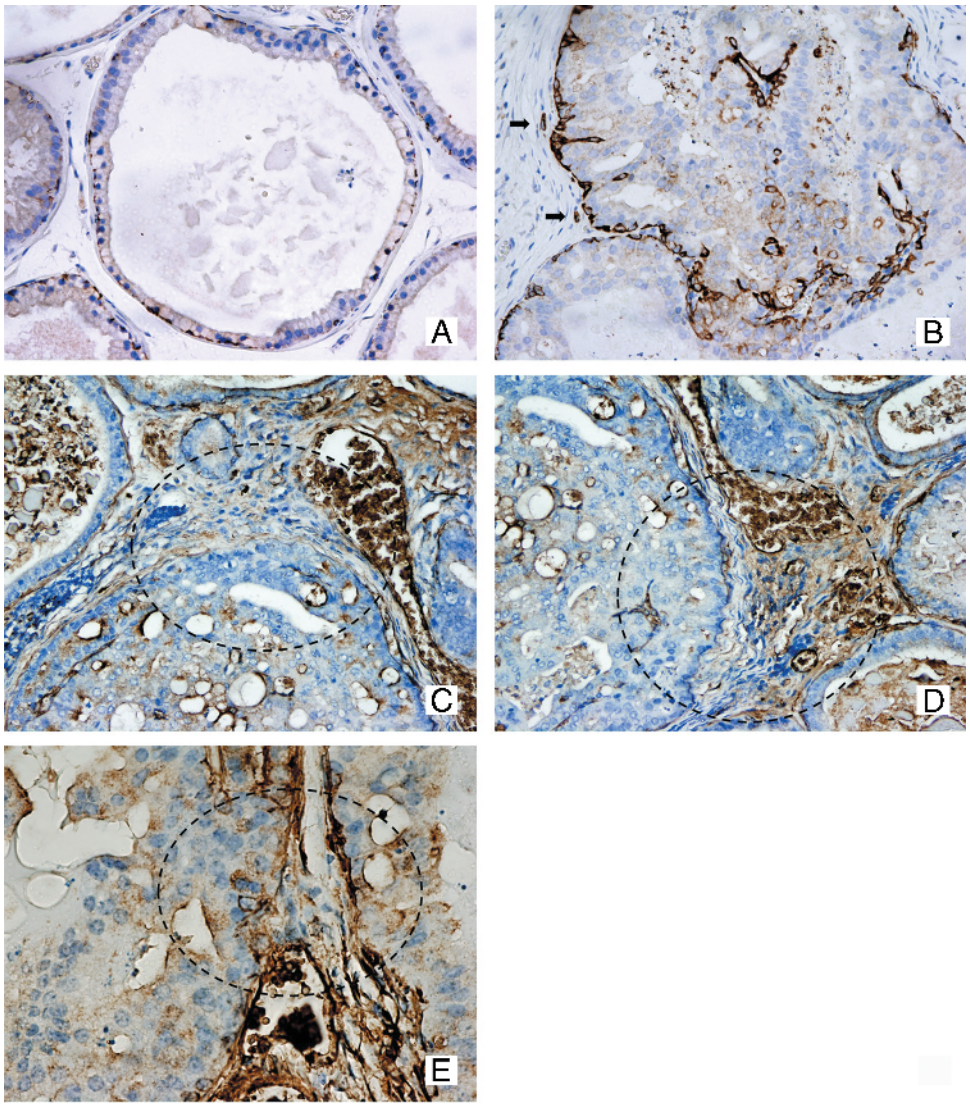

Figure W5. IHC staining for K14 and laminin in tissue from the ventral prostate of the $ARR_2Pb.Stat3C \times PTEN^{+/-}$ mice. (A) K14 staining of a normal gland (WT mouse) denoting a basal cell staining. (B) K14 staining of an adenocarcinoma from an $ARR_2Pb.Stat3C \times PTEN^{+/-}$ mouse. K14 was largely expressed in basal cells and in cells infiltrating the lumen of the neoplastic gland. In addition, K14 was expressed in some cells found in the stroma (arrows). (C–E) Laminin staining: pictures show a clear membrane disruption and adjacent invasion in the affected glands (circles).

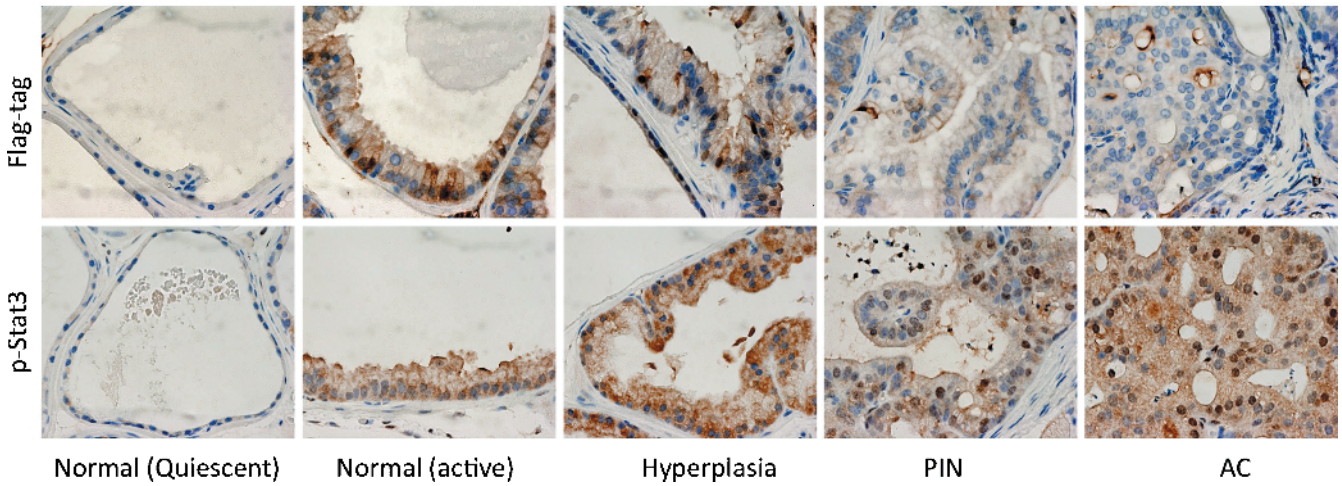

Figure W6. Composite picture showing IHC staining for the transgene (Stat3C) using antibodies to the Flag-tag and for phospho-Stat3 (using antibodies for phospho-Tyr^{705}) in normal glands (both quiescent and active), hyperplasia, PIN, and ACs from ventral prostate of the $ARR_2Pb.Stat3C \times PTEN^{+/-}$ mice. Stat3C was expressed in the normal (active) glands and hyperplastic glands from the ventral prostate of double transgenic mice. Staining was seen in both the cytoplasm and nucleus. Transgene expression (both cytoplasmic and nuclear) was reduced in both PIN and ACs. In contrast, phospho-Stat3 (Tyr^{705}) was primarily cytoplasmic in normal (active) and hyperplastic glands with strong nuclear staining in PIN and ACs.

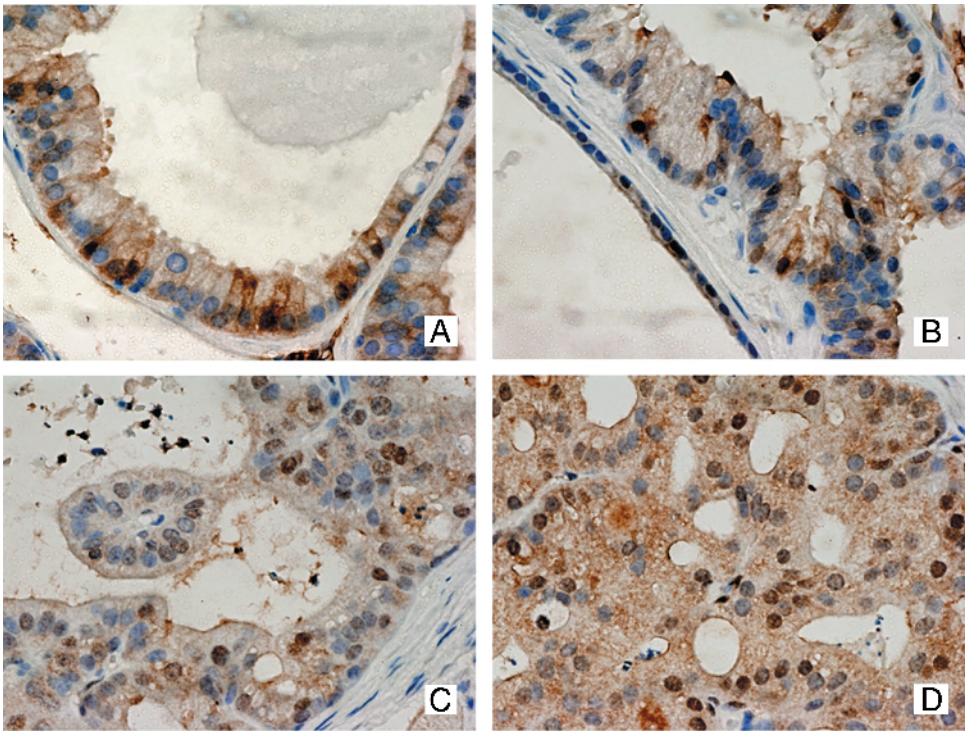

Figure W7. Higher magnification (×40) from the previous composite images of Flag-tag (Stat3C) staining in normal (active) and hyperplastic glands (A and B) and nuclear phospho-Stat3 staining in PIN and adenocarcinomas (C and D).

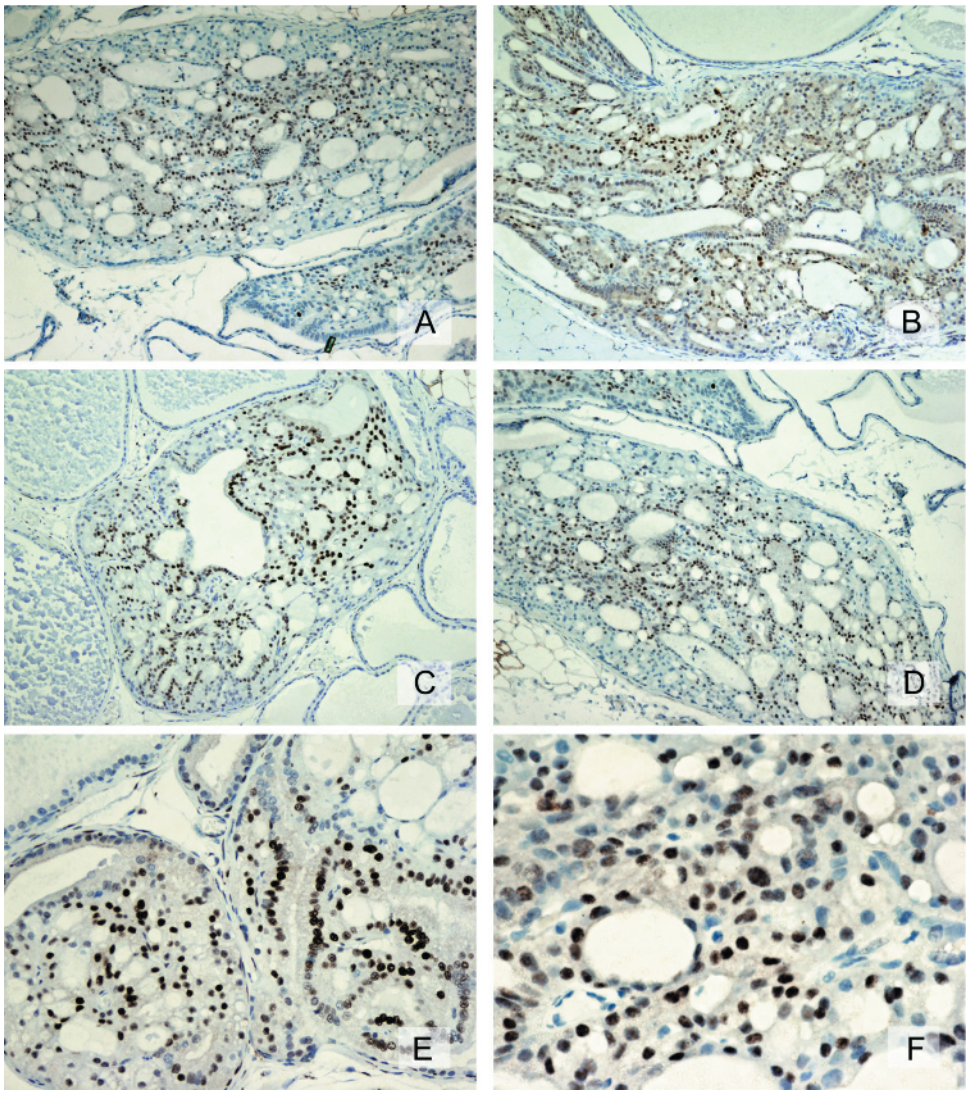

Figure W8. Additional IHC analyses of VP from 6- and 12-month-old $ARR_2Pb.Stat3C \times PTEN^{+/-}$ transgenic mice ($n = 5$) for phospho-NF-κB (p65). Strong nuclear staining was observed in 100% (5/5 samples) of the adenocarcinomas from the double transgenic mice. (A–D) Samples from four different mice (magnification, ×10). (E) Sample from another double transgenic mouse (magnification, ×20). (F) Higher magnification (magnification, ×40) of the same sample shown in panel D.